Since January 2020 Elsevier has created a COVID-19 resource centre with free information in English and Mandarin on the novel coronavirus COVID-19. The COVID-19 resource centre is hosted on Elsevier Connect, the company's public news and information website.

Article

Cell Host & Microbe

Robust SARS-CoV-2 infection in nasal turbinates after treatment with systemic neutralizing antibodies

Graphical Abstract

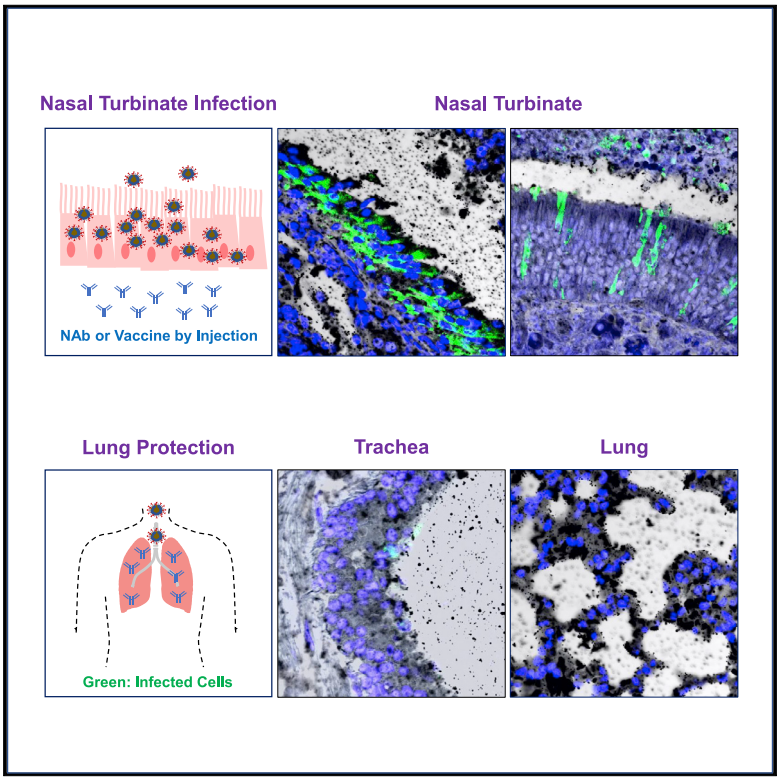

Highlights

- Systemic HuNAb or vaccine fails full SARS-CoV-2 infection prevention in nasal turbinate
- Post-exposure HuNAb suppresses SARS-CoV-2 in lungs but poorly in nasal turbinate
- Live SARS-CoV-2 persists in nasal turbinate for several days despite systemic HuNAb
- Robust SARS-CoV-2 infection in nasal turbinate is a mode to evade systemic HuNAb

Authors

Dongyan Zhou, Jasper Fuk-Woo Chan, Biao Zhou, ..., David D. Ho, Kwok-Yung Yuen, Zhiwei Chen

Correspondence

kyyuen@hku.hk (K.-Y.Y.), zchenai@hku.hk (Z.C.)

In brief

SARS-CoV-2 infection in nasal turbinate determines viral transmissibility. Zhou and colleagues interrogate site-specific prevention of SARS-CoV-2 in hamsters. Prophylactic intraperitoneal or intranasal HuNAb or intramuscular DNA vaccination prevents infection effectively in lungs but not in nasal turbinate. Rapid postchallenge HuNAb suppresses infection significantly in lungs but poorly in nasal turbinate.

Zhou et al., 2021, Cell Host & Microbe *29*, 1–13
April 14, 2021
https://doi.org/10.1016/j.chom.2021.02.019

CellPress

Cell Host & Microbe

CellPress

Article

Robust SARS-CoV-2 infection in nasal turbinates after treatment with systemic neutralizing antibodies

Dongyan Zhou,[1,3,8] Jasper Fuk-Woo Chan,[2,3,4,5,8] Biao Zhou,[1,3,8] Runhong Zhou,[1,3,8] Shuang Li,[1,3,8] Sisi Shan,[6,8] Li Liu,[1,3,8] Anna Jinxia Zhang,[2,3,4] Serena J. Chen,[1,2] Chris Chung-Sing Chan,[2,3] Haoran Xu,[1,3] Vincent Kwok-Man Poon,[2,3] Shuofeng Yuan,[2,3,4,5] Cun Li,[2,3] Kenn Ka-Heng Chik,[2,3] Chris Chun-Yiu Chan,[2,3] Jianli Cao,[2,3] Chun-Yin Chan,[1,3] Ka-Yi Kwan,[1,3] Zhenglong Du,[1,3] Thomas Tsz-Kan Lau,[1,3] Qi Zhang,[6] Jie Zhou,[2,3,4] Kelvin Kai-Wang To,[2,3,4,5] Linqi Zhang,[6] David D. Ho,[7] Kwok-Yung Yuen,[2,3,4,5,*] and Zhiwei Chen[1,2,3,5,9,*]

[1]AIDS Institute, Li Ka Shing Faculty of Medicine, the University of Hong Kong, Pokfulam, Hong Kong SAR, PRC
[2]State Key Laboratory of Emerging Infectious Diseases, the University of Hong Kong, Pokfulam, Hong Kong SAR, PRC
[3]Department of Microbiology, Li Ka Shing Faculty of Medicine, the University of Hong Kong, Pokfulam, Hong Kong SAR, PRC
[4]Carol Yu Center for Infection, The University of Hong Kong, Pokfulam, Hong Kong SAR, PRC
[5]Department of Clinical Microbiology and Infection Control, the University of Hong Kong-Shenzhen Hospital, Shenzhen, Guangdong, PRC
[6]Center for Global Health and Infectious Diseases, Comprehensive AIDS Research Center and School of Medicine, and Vanke School of Public Health, Tsinghua University, Beijing, PRC
[7]Aaron Diamond AIDS Research Center, Columbia University Vagelos College of Physicians and Surgeons, New York, NY 10032, USA
[8]These authors contributed equally
[9]Lead contact
*Correspondence: kyyuen@hku.hk (K.-Y.Y.), zchenai@hku.hk (Z.C.)
https://doi.org/10.1016/j.chom.2021.02.019

SUMMARY

Severe acute respiratory syndrome coronavirus 2 (SARS-CoV-2) is characterized by a burst in the upper respiratory portal for high transmissibility. To determine human neutralizing antibodies (HuNAbs) for entry protection, we tested three potent HuNAbs (IC_{50} range, 0.0007–0.35 μg/mL) against live SARS-CoV-2 infection in the golden Syrian hamster model. These HuNAbs inhibit SARS-CoV-2 infection by competing with human angiotensin converting enzyme-2 for binding to the viral receptor binding domain (RBD). Prophylactic intraperitoneal or intranasal injection of individual HuNAb or DNA vaccination significantly reduces infection in the lungs but not in the nasal turbinates of hamsters intranasally challenged with SARS-CoV-2. Although post-challenge HuNAb therapy suppresses viral loads and lung damage, robust infection is observed in nasal turbinates treated within 1–3 days. Our findings demonstrate that systemic HuNAb suppresses SARS-CoV-2 replication and injury in lungs; however, robust viral infection in nasal turbinate may outcompete the antibody with significant implications to subprotection, reinfection, and vaccine.

INTRODUCTION

Severe acute respiratory syndrome coronavirus 2 (SARS-CoV-2) has resulted in about 80 million infections globally with nearly 1.7 million deaths by the end of 2020 since the discovery of the disease outbreak in December 2019 (Chan et al., 2020d; Zhu et al., 2020). The growing coronavirus disease 2019 (COVID-19) pandemic urgently requires the development of effective prophylaxis and treatment. While triple combination therapy (interferon-β1b, lopinavir/ritonavir, and ribavirin), remdesivir, and dexamethasone have all shown some clinical benefits in select patient groups (Boulware et al., 2020; Goldman et al., 2020; Hung et al., 2020b), the discovery of specific anti-SARS-CoV-2 agents with higher efficacy, better safety profiles, and bioavailability remain essential for improving the clinical outcome of COVID-19 patients. In addition to some drugs identified in large-scale drug repurposing programs (Riva et al., 2020), direct cloning of human neutralizing antibodies (HuNAbs) against SARS-CoV-2 has also been reported recently (Cao et al., 2020; Liu et al., 2020b; Robbiani et al., 2020; Shi et al., 2020; Sun et al., 2020; Wu et al., 2020a, 2020b; Zost et al., 2020). Furthermore, with the recent clinical trials of HuNAbs and urgent approval of COVID-19 vaccines for human use, it is necessary to determine whether or not HuNAbs may warrant sterile protection against live SARS-CoV-2 infection.

Unlike SARS patients who had peak upper respiratory tract (URT) viral loads at day 10 after symptom onset (Peiris et al., 2003), COVID-19 patients exhibited peak salivary or URT viral loads during the first week after symptom onset that declined over time; this phenomenon could account for the fast-spreading nature of the pandemic (Hung et al.,

Please cite this article in press as: Zhou et al., Robust SARS-CoV-2 infection in nasal turbinates after treatment with systemic neutralizing antibodies, Cell Host & Microbe (2021), https://doi.org/10.1016/j.chom.2021.02.019

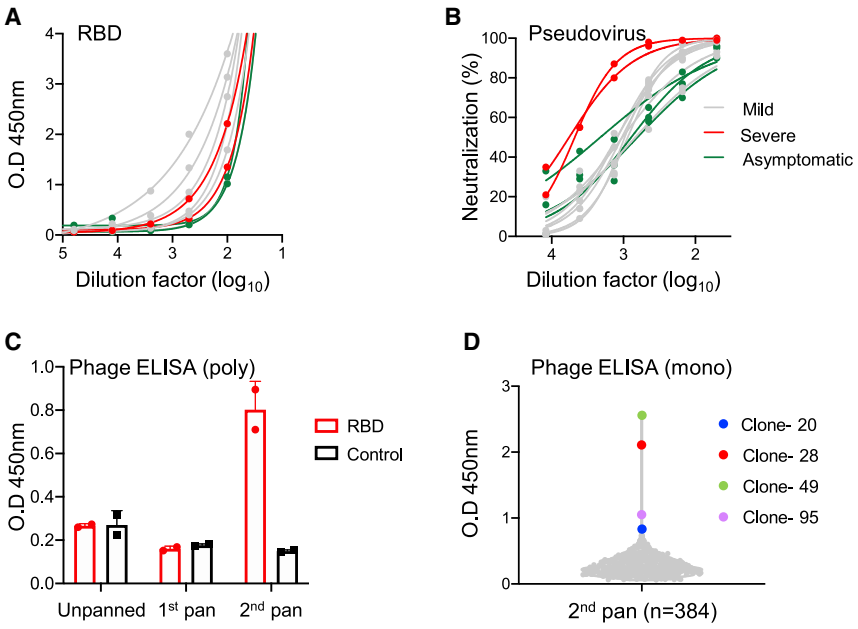

Figure 1. Screening of SARS-CoV-2 neutralizing antibodies from convalescent patients

(A) Humoral immune responses to SARS-CoV-2 were analyzed in each patient by endpoint ELISA for binding to viral RBD.

(B) The pseudovirus assay was used to measure neutralization activity. Color-coded lines showed antibody responses from patients categorized according to disease severity.

(C and D) A phage-displayed antibody Fab library (C) and monoclonal phage colonies (D) were tested against RBD by ELISA throughout the panning procedure. Unpanned phage library, first round and second round amplified phage polyclones (poly) were tested at a 1:5 dilution by phage ELISA. An unrelated antigen was used as a control. A total of 384 single colonies (mono) were picked and verified for binding with RBD by ELISA. The four strongest single-phage binders were color coded and named according to the clone numbers.

See also Figures S1–S3 and Tables S1, S2, and S7.

2020a; To et al., 2020b). Regarding the humoral response, SARS-CoV-2-specific IgG and neutralizing antibody responses were quickly detectable in adult and children patients only 6 days after symptom onset (Liu et al., 2020c; Suthar et al., 2020; Zhou et al., 2020b). However, COVID-19 patients with higher amounts of anti-spike (S) and anti-nucleocapsid (NP) IgM and IgG tend to have poorer disease outcomes (Jiang et al., 2020; Tan et al., 2020). We and others also reported that COVID-19 patients with severe disease developed significantly more robust SARS-CoV-2-specific NAb responses (Liu et al., 2020a; Wang et al., 2020a, 2020b). Nevertheless, convalescent plasma with high NAb titers from recovered patients has been reported to be beneficial in the treatment of severe COVID-19 in small case cohorts (Duan et al., 2020). To replace convalescent plasma, which is not readily available in most countries, HuNAbs have been recently identified and showed promising results in preclinical studies (Cao et al., 2020; Liu et al., 2020b; Robbiani et al., 2020; Shi et al., 2020; Sun et al., 2020; Wu et al., 2020a, 2020b; Zost et al., 2020). However, the *in vivo* efficacy of anti-SARS-CoV-2 HuNAbs in protecting against URT infection in a physiologically relevant animal model has not been thoroughly investigated.

In this study, we identified a panel of candidate HuNAbs and conducted a thorough investigation of the lead candidate HuNAb ZDY20 at a dose of 10 mg/kg, which is much higher than its IC_{50} and IC_{90} values of 0.35 and 1 μg/mL, respectively, against live SARS-CoV-2 infection in both prophylactic and therapeutic settings in our established golden Syrian hamster model for COVID-19 (Chan et al., 2020a). We also tested the prophylactic efficacy of two much stronger RBD-specific HuNAbs 2–15 (IC_{50} and IC_{90} values of 0.0007 and 0.04 μg/mL) and ZB8 (IC_{50} and IC_{90} values of 0.013 and 0.031 μg/mL) and an S-based DNA vaccine to address the possible sterile protection in the same animal model.

RESULTS

Generation of a phage library displaying human antibody Fab of COVID-19 patients

To clone SARS-CoV-2-specific HuNAbs, we obtained peripheral blood mononuclear cells (PBMCs) from 12 convalescent COVID-19 patients in Hong Kong at a mean duration of 19 (±10.4) days after symptom onset (Table S1). These patients included seven females and five males with a mean age of 59 years (range, 21–75). Two patients had severe disease, seven had mild disease, and three were asymptomatic. The PBMCs of these 12 patients were pooled for the generation of a Fab phage library, as only small amounts of PBMCs were obtained from each patient. ELISA and pseudovirus neutralization assays were performed to measure the antibody titers in each patient's serum prior to pooling, which confirmed that each study subject had SARS-CoV-2 RBD-specific binding (Figure 1A) and neutralizing antibody activities (Figure 1B). Consistent with the observations that we and others reported previously, the two severe patients had higher NAb titers than the mild and asymptomatic patients (Liu et al., 2020a; Riva et al., 2020; Wang et al., 2020a). The mean NAb IC_{50} titer was 1:1753 with a range of 1:638–1:5701 (Figure 1B). Using the pooled PBMCs, we first set up a Fab phage library consisting of 3×10^6 clones (Figure S1). We subsequently developed an in-solution selection method for two rounds of panning (Figure 1C). We were able to pick up 384 single reactive colonies (Figure 1D). Next, we tested the binding ability of phage-displayed Fab to recombinant SARS-CoV-2 RBD by a monoclonal phage-based ELISA followed by sequencing 18 single-phage colonies that displayed strong RBD-binding ability. Finally, we obtained four pairs of variable heavy (VH) chain/variable light (VL) chain from the top four clones (Figure 1D, color-coded), which resulted in four human monoclonal antibodies in the native form of IgG1, named ZDY20, ZDY28, ZDY49, and ZDY95.

Please cite this article in press as: Zhou et al., Robust SARS-CoV-2 infection in nasal turbinates after treatment with systemic neutralizing antibodies, Cell Host & Microbe (2021), https://doi.org/10.1016/j.chom.2021.02.019

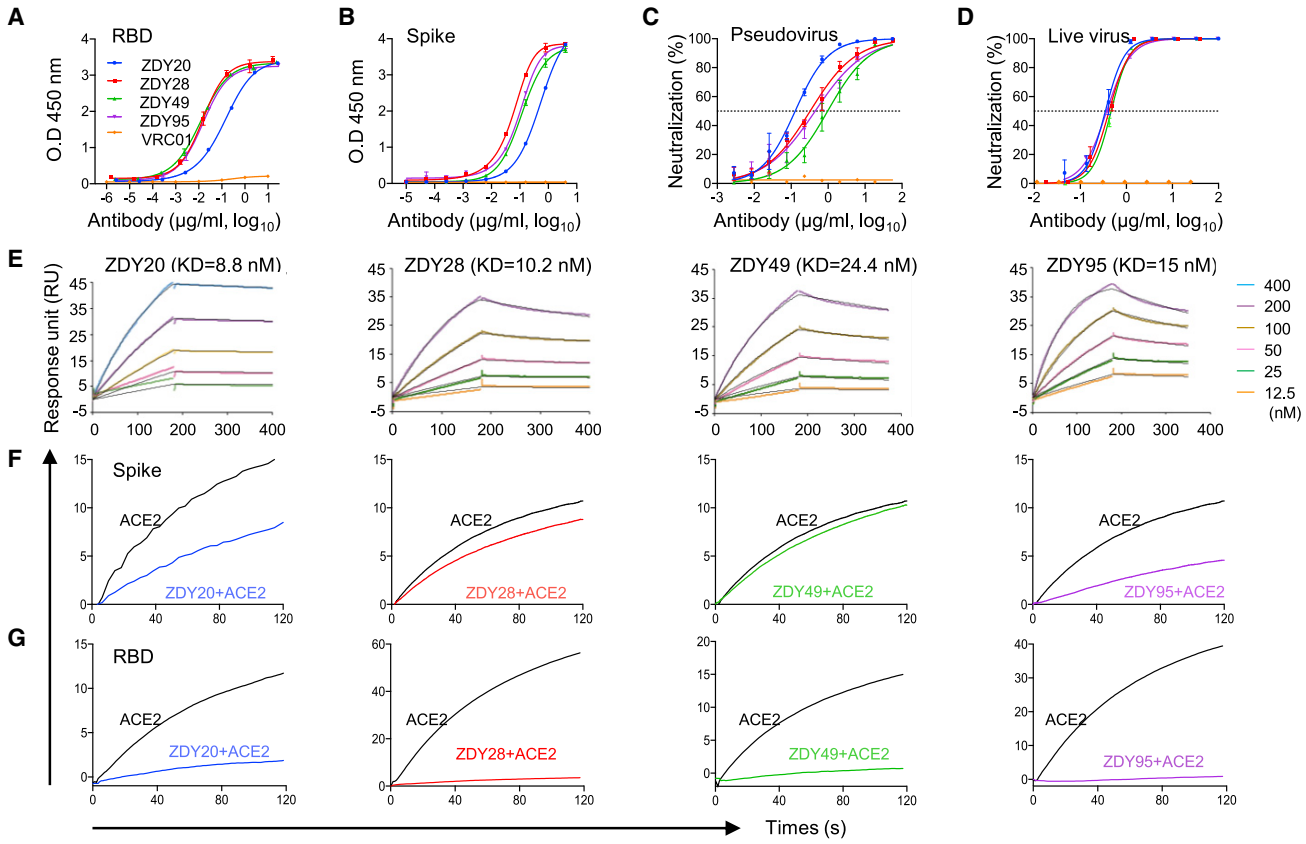

Figure 2. *In vitro* characterization of SARS-CoV-2-specific HuNAbs

(A) Binding profiles of four color-coded candidate HuNAbs (ZDY20, 28, 49, and 95) to viral RBD were determined. HIV-1-specific HuNAb VRC01 served as a negative control.

(B) Binding profiles of four HuNAbs to viral SARS-CoV-2 spike trimer were also determined.

(C) Neutralization activities of four candidate HuNAbs were tested against pseudovirus in 293T-ACE2 cells.

(D) Four candidate HuNAbs were also tested against live SARS-CoV-2 in Vero-E6 cells. Both neutralization assays were performed in triplicate wells, and the results are shown as the mean ± SEM.

(E) Binding kinetics of four candidate HuNAbs to SARS-CoV-2 spike trimer protein by the SPR. The black lines indicate the experimentally derived curves, whereas the colored lines represent fitted curves from serially diluted antibody concentrations injected in the experiment. The KD results are representative of two independent experiments.

(F and G) HuNAb competition with ACE2 for binding to SARS-CoV-2 spike trimer (F) and soluble RBD (G) measured by the SPR. The plots show distinct binding patterns of ACE2 to the spike or RBD protein with (colored curve) or without (black curve) prior incubation with each tested HuNAb. The results are representative of two independent experiments and color coded for each HuNAb.

See also Tables S3 and S4.

Specificity and neutralizing activities of cloned HuNAbs against SARS-CoV-2

Sequence analysis revealed that ZDY28, ZDY49, and ZDY95 share high similarity with the same immunoglobulin heavy chain variable region gene 3-30 (IGHV3-30) and immunoglobulin kappa chain variable region gene 1-39 (IGKV1-39) (Table S2). They share identical complementarity-determining region 3 (CDR3) heavy (H) and CDR3 light (L) chains but with a few amino acid differences in framework region 1 (FR1) (Figure S2). Since repeated sequencing gave identical results and the IGHV/IGKV fragments were cloned from the phage library derived from 12 patients, it is possible that the small amino acid differences between ZDY49 and ZDY95 might be derived from different donors. In contrast, ZDY20 has IGHV3-53 and IGKV1-33, which were recently shown to be associated with higher antiviral activity (Dalamaga et al., 2020; Yuan et al., 2020). ZDY20 has a longer $CDR3_H$ with three additional amino acids compared with the other three antibodies (Figure S2). These four antibodies all had low rates of somatic hypermutation (SHM) in both IGHV (0.35% or 0.69%) and IGKV (0.36% or 1.08%), except that the SHM rate in IGKV of ZDY20 reached 7.89% (Table S2). We next analyzed the binding activity of these four antibodies to recombinant SARS-CoV-2 RBD and S proteins by ELISA. In these solid phase ELISAs, ZDY28, ZDY49, and ZDY95 showed similar binding abilities to RBD (EC_{50} 0.012 μg/mL) (Figure 2A) and to S (EC_{50} 0.1 μg/mL) (Figure 2B), which were lower than those of ZDY20 (EC_{50} 0.135 and 0.52 μg/mL, respectively) (Table S3). However, the anti-SARS-CoV-2 neutralization activity of ZDY20 (IC_{90} 1.24 μg/mL) was better than those of ZDY28 (IC_{90} 7.47 μg/mL), ZDY49 (IC_{90} 17.08 μg/mL), and ZDY95 (IC_{90} 13.35 μg/mL) in the pseudovirus assay (Figure 2C; Table S3). Moreover, ZDY20 exhibited, relatively, a better IC_{90} (1 μg/mL) than those of ZDY28 (1.28 μg/mL), ZDY49 (1.24 μg/mL), and

Please cite this article in press as: Zhou et al., Robust SARS-CoV-2 infection in nasal turbinates after treatment with systemic neutralizing antibodies, Cell Host & Microbe (2021), https://doi.org/10.1016/j.chom.2021.02.019

ZDY95 (1.5 μg/mL) against live SARS-CoV-2 in Vero-E6 cells (Figure 2D; Table S3). Notably, none of these HuNAbs showed cross-neutralization against the SARS-CoV pseudovirus (data not shown). Using a random yeast surface display of SARS-CoV-2 S fragments, we observed that all four HuNAbs recognized conformational determinants instead of a small linear epitope because their binding domain on viral RBD required a minimum of 179 amino acid residues (337–524 for ZDY20, 336–523 for ZDY28, and 336–515 for ZDY49 and ZDY95) (Figure S3). Next, we measured the binding affinity of each antibody to the SARS-CoV-2 RBD or S trimer using surface plasmon resonance (SPR). Similar to the weaker binding activity observed by ELISA, ZDY20 Fab showed weaker affinity binding to SARS-CoV-2 RBD with a KD value of 74.9 nM, which was larger than those of the other three antibodies (ZDY28 19.2 nM, ZDY49 42.3 nM, and ZDY95 26.2 nM) (Table S4). The complete ZDY20 antibody, however, displayed the highest avidity binding to SARS-CoV-2 S trimer with a dissociation constant (KD) value of 8.8 nM, which was lower than those of the other three antibodies (ZDY28 10.2 nM, ZDY49 24.4 nM, and ZDY95 15 nM) (Figure 2E; Table S4). Furthermore, in the human cellular receptor angiotensin converting enzyme-2 (ACE2) competition assay by SPR, ZDY20 presented the most potent activity to block S binding to ACE2 followed by ZDY95, ZDY28, and ZDY49 (Figure 2F), although ZDY20 was not the strongest competitor to block soluble RBD binding to ACE2 (Figure 2G). These results suggested that the relative higher anti-SARS-CoV-2 neutralizing potency of ZDY20 is likely due to its stronger competitive blockade of S trimer binding to ACE2, which is probably associated with avidity interaction. Based on its relatively better activities of avidity binding KD to S, blocking S binding to ACE2, and neutralization, we chose ZDY20 for subsequent *in vivo* experiments.

SARS-CoV-2 robustly infects nasal turbinate despite systemic ZDY20 prophylaxis as compared with two stronger HuNAbs and DNA vaccination

To determine the potential role of HuNAb as prophylaxis for SARS-CoV-2 infection, we first administered ZDY20 intraperitoneally to golden Syrian hamsters before virus challenge in our biosafety level-3 (BSL-3) animal laboratory. Syrian hamsters typically recover from SARS-CoV-2 infection with resolution of clinical signs and clearance of virus shedding within 1 week after infection, as we previously described (Chan et al., 2020a). Accordingly, the hamsters were sacrificed for analysis at 4 days post-infection (dpi) when high viral loads and acute lung injury were consistently observed. In this prophylaxis study, each hamster received a single intraperitoneal injection of either 10 mg/kg (n = 4) high dose or 5 mg/kg (n = 3) low dose of ZDY20 (Figure 3A) that were much higher than its IC_{90} value of 1 μg/mL tested by live SARS-CoV-2 in Vero-E6 cells, respectively. Another group of hamsters (n = 4) was injected with a control HIV-1-specific HuNAb VRC01 at a high dose of 10 mg/kg (Liu et al., 2020b). Twenty-four hours after the ZDY20 injection, each animal was challenged intranasally with 10^5 plaque-forming units (PFUs) of live SARS-CoV-2 (HKU-001a strain) (Chan et al., 2020a; Liu et al., 2020b). At 4 dpi, nasal turbinate, trachea, and lung tissues were harvested to quantify infectious viruses by plaque assay, viral loads by real-time PCR and infected cells by immunofluorescence (IF) staining. We found that infectious PFUs were readily detected in all tissue compartments of VRC01-controlled hamsters tested but not in 75% and 0% nasal turbinates, 75% and 67% trachea, and 50% and 33% lungs of hamsters that were given high and low doses of ZDY20, respectively (Figure 3B). The more sensitive RT-PCR further demonstrated that viral RNA copy numbers were reduced in the lungs by an average of 3 logs (range, 0.7–4.5) (Figure 3C). In contrast, there was no significant viral load reduction in nasal turbinates and trachea in both dose groups, suggesting less preventive efficacy by ZDY20 in the URT of viral entry. To determine the role of ZDY20 in protection, we measured the serum antibody concentration and neutralization titer at 0 and 4 dpi. Over 40 and 9 μg/mL ZDY20 were found in 50% high-dose and 67% low-dose animals at 0 dpi (Figure 3D, solid symbol; Table S5), together with mean IC_{50} values of approximately 1:236 and 1:99, respectively (Figure 3E, solid symbol). At 4 dpi, over 26 and 5 μg/mL ZDY20 were found in 50% high-dose and 67% low-dose animals (Figure 3D, open symbol; Table S5), together with mean IC_{50} values of approximately 1:55 and 1:45, respectively (Figure 3E, open symbol). These results demonstrated that most animals maintained peripheral amounts of ZDY20 much higher than its IC_{90} values during the entire course of the experiment.

Next, to understand whether or not ZDY20 protects against infection-induced lung injury in hamsters, we performed pathological analysis on lung specimens. Compared with uninfected healthy animals (Figure S4), hamsters treated with the high-dose ZDY20 showed mild interstitial alveoli inflammation with minor septal infiltration and congestion (Figure 3F, top left, arrows). There was no apparent peribronchiolar infiltration, and the bronchiolar epithelia appeared normal (open arrows). Hamsters treated with the low dose showed limited areas of bronchiolar epithelial cell swelling and detachment (Figure 3F, middle left, open arrows) together with mild peribronchiolar infiltration and mild alveolar septal infiltration. In contrast, control hamsters showed large patchy areas of alveolar wall and alveolar space involvement by inflammatory infiltrates and exudation (Figure 3F, bottom left, arrows). The two blood vessels (BVs) in the lung section showed vasculitis and endotheliitis. Furthermore, we performed IF staining of viral NP antigen in both lung and nasal turbinate tissues compared with uninfected healthy animals (Figure S4). In the high-dose group, little viral NP expression was observed in lung sections (Figure 3F, top right). In the low-dose group, a small amount of viral NP was observed in localized areas of alveoli (Figure 3F, middle right, arrows) and in the epithelia of a few bronchiolar sections (thin arrows). In contrast, control hamsters showed diffuse NP expression in extensive areas of alveoli (Figure 3F, bottom right, thick arrows) and in the bronchiolar epithelia (thin arrows). The mean number of NP^+ cells per 50×field in the lungs was significantly lower in the high-dose group than that in the control animals (Figure 3G). Remarkably, nasal turbinate tissues showed damage to the respiratory and olfactory epithelium with extensive submucosal immune cell infiltration, together with robust and diffuse viral NP expression in extensive areas lining the stratified squamous epithelia in both the high-dose and low-dose groups of ZDY20-treated animals, similar to untreated control hamsters (Figures 4A–4C). Moreover, no significant difference in NP^+ cells per 50×field was found between treated and control animals when nasal turbinate tissues were analyzed (Figure 4D). Collectively, these results demonstrated that prior administration of 10 mg/kg ZDY20 did not prevent robust SARS-CoV-2 infection

Please cite this article in press as: Zhou et al., Robust SARS-CoV-2 infection in nasal turbinates after treatment with systemic neutralizing antibodies, Cell Host & Microbe (2021), https://doi.org/10.1016/j.chom.2021.02.019

CellPress

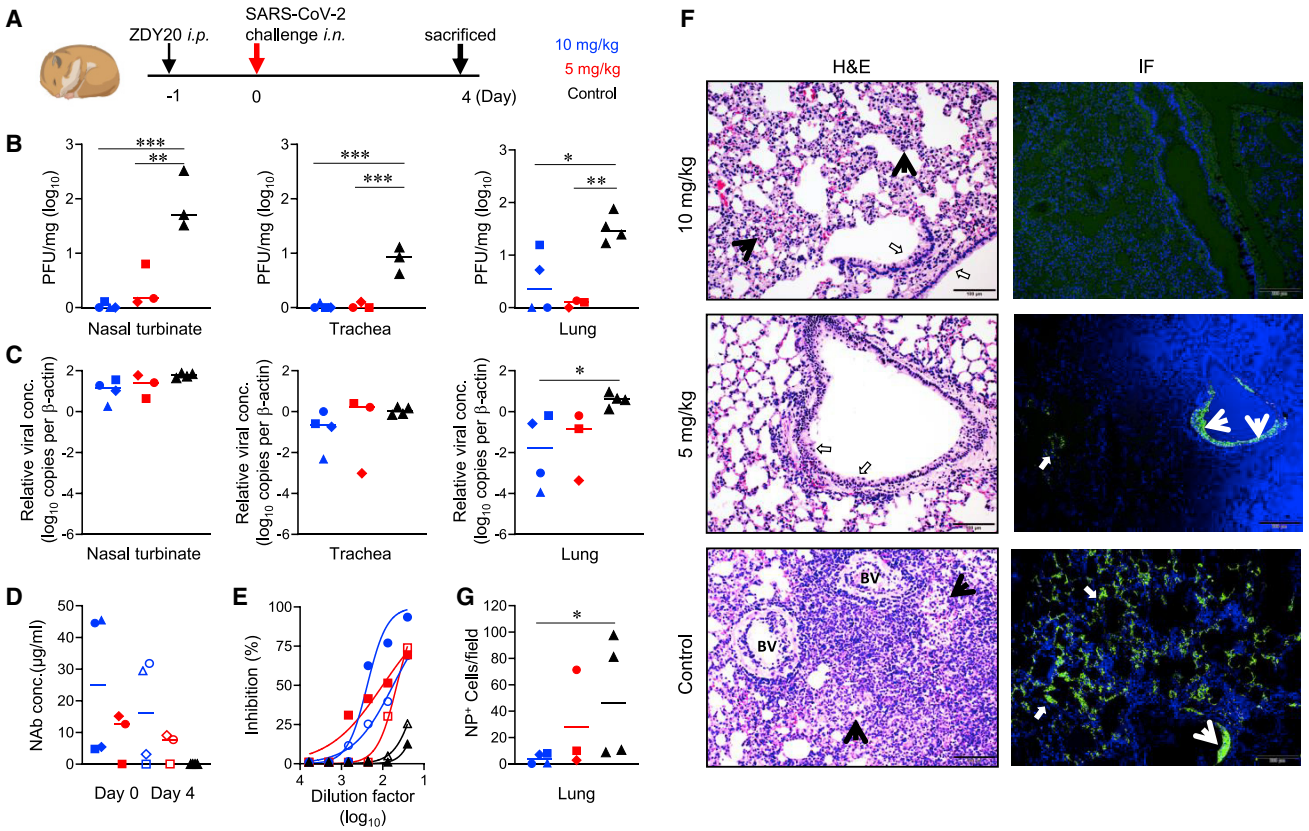

Figure 3. Efficacy of ZDY20 prophylaxis against live SARS-CoV-2 in Syrian hamsters

(A) Experimental schedule and color coding for three experimental groups. Two groups of hamsters received a single intraperitoneal injection of ZDY20 at doses of 10 mg/kg (n = 4) and 5 mg/kg (n = 3) one day before the live virus challenge (−1 dpi). Another group was given the control antibody VRC01 at 10 mg/kg (n = 4). On day 0, each hamster was intranasally inoculated with a challenge dose of 100 μL of Dulbecco's modified Eagle medium containing 10^5 plaque-forming units of SARS-CoV-2 (HKU-001a strain, GenBank accession no: MT230904.1). The hamsters were sacrificed at 4 dpi for analysis.

(B) Infectious virions were tested by viral plaque assay in nasal turbinate, trachea, and lung tissue homogenates. PFUs per mg of tissue extractions were compared between different groups in $\log_{10}$-transformed units.

(C) The relative viral concentration (normalized by β-actin) was determined in nasal turbinate, trachea, and lung tissue homogenates by the sensitive RT-PCR assay.

(D and E) Serum concentration (D) and neutralizing activity (E) of HuNAb ZDY20 were determined by ELISA and pseudovirus assays, respectively. Open symbols represent corresponding samples collected at 4 dpi in the same color-coding groups.

(F) Representative images of hamster lung tissues by H&E (100×, left panel) and immunofluorescence (IF) staining (50×, right panel). For viral NP antigen in the sections (50×) stained by IF, the lungs of control hamsters showed diffuse NP expression in large areas of alveoli (thick arrows) and in bronchiolar epithelium (thin arrows). SARS-CoV-2 N protein (NP) was stained green, and cell nuclei were counterstained with DAPI (blue). No NP expression was observed in lung sections of hamsters treated with high-dose antibody (10 mg/kg). In low-dose antibody-treated hamsters, NP expression was occasionally observed in a small area of alveoli (thick arrows) and in the epithelium of a few bronchiolar sections (thin arrows).

(G) NP^+ cells per 50×field were compared in the lungs of three experimental groups. Data of individual animals were indicated by different symbols, and different colors represented different groups. Statistics were generated using ordinary one-way ANOVA and multiple comparisons test. *$p < 0.05$; **$p < 0.01$; ***$p < 0.001$. See also Figures S4 and S9 and Table S5.

in nasal turbinates but suppressed productive infection in lungs in the Syrian hamster model.

Considering that HuNAbs with greater inhibitory potency may be more effective in preventing viral replication in the nasal turbinates, we tested two such RBD-specific HuNAbs, namely ZB8 and 2-15. ZB8 is a newly cloned HuNAb with IC_{50} and IC_{90} values of 0.013 and 0.031 μg/mL, whereas 2-15 has been previously reported with IC_{50} and IC_{90} values of 0.0007 and 0.04 μg/mL, all in the live virus neutralization assay (Table S6) (Liu et al., 2020b). ZB8 and 2-15 are therefore up to 32-fold (IC_{90}) to 500-fold (IC_{50}) stronger than ZDY20. Prophylactic intraperitoneal injection of 4.5 mg/kg ZB8 and 1.5 mg/kg 2-15 were tested in hamsters using the same protocol as ZDY20. We consistently observed significantly reduced viral loads and NP^+ cells in the lungs, but not in nasal turbinates, of experimental hamsters at 4 dpi in both experiments (Figures 5A, 5B, S5, and S6). We subsequently tested prophylactic intranasal inoculation of 10 mg/kg ZDY20 and 4.5 mg/kg ZB8, respectively, followed by the same viral challenge at 12 h post-antibody intervention (Figures 5C and S7). Surprisingly, we observed significantly reduced infectious PFUs and viral loads in lungs mainly by ZB8 but still not in nasal turbinates of experimental hamsters at 4 dpi in both experiments. Abundant NP^+ cells were readily found in nasal turbinate of each treated animal. In addition, we examined the efficacy of a systemic DNA vaccine that was

Please cite this article in press as: Zhou et al., Robust SARS-CoV-2 infection in nasal turbinates after treatment with systemic neutralizing antibodies, Cell Host & Microbe (2021), https://doi.org/10.1016/j.chom.2021.02.019

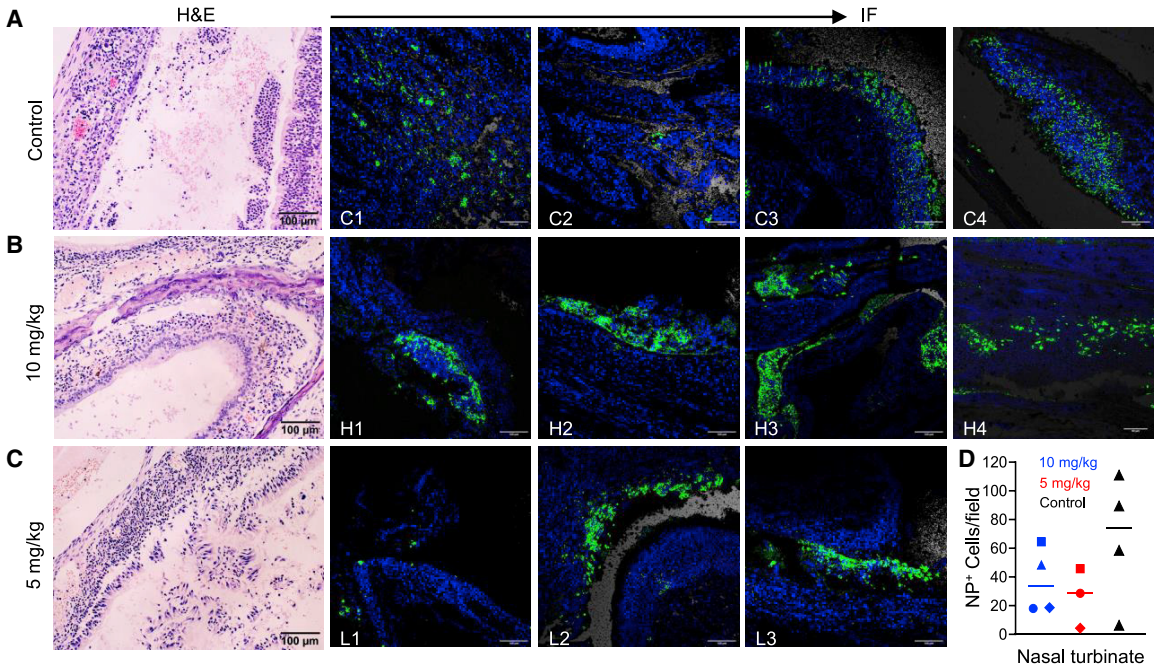

Figure 4. Robust SARS-CoV-2 infection in nasal turbinates at 4 dpi in the HuNAb ZDY20 prophylaxis experiment by H&E and IF staining

(A) H&E staining showed that both the respiratory epithelium (left) and olfactory epithelium (right) are affected by extensive submucosal infiltration and epithelial cell death, resulting in loss of the whole surface layer of epithelial cells. The nasal cavity contains exudates mixed with red blood cells and immune cells. The images of IF staining showed the abundancy and distribution of NP^+ cells in the nasal turbinates of each control animal (C1-4). SARS-CoV-2 N protein (NP) was stained green, and cell nuclei were counterstained with DAPI (blue).

(B) H&E staining showed submucosal immune cell infiltration and a large amount of epithelial cell desquamation. The images of IF staining showed the abundancy and distribution of NP^+ cells in the nasal turbinates of each animal that received the high dose of 10 mg/kg ZDY20 (H1-4).

(C) Similarly, H&E staining showed submucosal immune cell infiltration and a large amount of epithelial cell desquamation. The images of IF staining showed the abundancy and distribution of NP^+ cells in the nasal turbinate of each animal that received the low dose of 5 mg/kg ZDY20 (L1-3).

(D) NP^+ cells per 50×field were compared in nasal turbinates of three animal groups. Data of individual animals were indicated by different symbols, and different colors represented different groups.

See also Figure S4.

codon-optimized and encoded the full-S protein as we previously described for SARS (Yi et al., 2005). The S protein was detected in transfected cells by western blot (Figures S8A and S8B) and presented with correct conformation by supporting pseudovirus infection (Liu et al., 2020a). Four injections of DNA vaccination induced both RBD binding and neutralizing antibodies in hamsters (Figures S8C–S8E). The mean NAb IC_{50} titer at 1 day before viral challenge sustained at 1:4419 with a range of 1:286–14175 comparable to most convalescent human subjects (Figure 1B) and vaccinees (Sadoff et al., 2021; Sahin et al., 2020; Xia et al., 2020). After the intranasal challenge, significantly reduced viral loads and NP^+ cells were observed in the lungs but not in nasal turbinates of hamsters at 4 dpi (Figures 5D and S8F–S8H). Our results therefore demonstrated that passive immunization and intramuscular DNA vaccination tested are unlikely effective for mucosal sterile protection due to robust viral infection in nasal turbinates outcompeting the systemic neutralizing antibodies.

Postchallenge ZDY20 therapy reduces SARS-CoV-2 infection in the lungs but considerably less in nasal turbinate

To explore the therapeutic potential of ZDY20, we infected four groups of hamsters (n = 4 per group) as described above. Three groups of hamsters were then treated intraperitoneally with a single high dose of 10 mg/kg at 1, 2, and 3 dpi (Figure 6A, color-coded). The fourth group was the VRC01 control using the same dose at 1 dpi. All animals were consistently sacrificed at 4 dpi for measurements of infectious virus titers and viral RNA copy numbers in lung, trachea, and nasal turbinate tissues (Figures 6B and 6C). At 1 dpi, ZDY20-treated hamsters showed no measurable infectious viruses in 100% nasal turbinates, 100% trachea, and 75% lungs by the plaque assay (Figure 6B, blue). The mean viral load reduction was 0.7 logs in both nasal turbinates (range, 0.1–1.0 logs) ($p < 0.05$) and trachea (range, 0.3–1.5 logs) but was 1.2 logs (range, 0.8–1.8 logs) in lungs ($p < 0.01$) compared with the control group (Figure 6C, blue). At 2 dpi, ZDY20-treated hamsters presented no measurable infectious viruses in 75% nasal turbinates, 75% trachea, and 50% lungs (Figure 6B, red). The mean viral load reduction was 1 log (range, 0.3–1.5 logs) in the trachea ($p < 0.05$) but not significant in the nasal turbinates and lungs compared with the control group (Figure 6C, red). At 3 dpi, ZDY20-treated hamsters had no measurable infectious viruses in 25% nasal turbinates, 75% trachea, and 25% lungs (Figure 6B, green). The mean viral load reduction was not significant in the nasal turbinates, trachea, or lungs compared with the control group (Figure 6C, green).

Please cite this article in press as: Zhou et al., Robust SARS-CoV-2 infection in nasal turbinates after treatment with systemic neutralizing antibodies, Cell Host & Microbe (2021), https://doi.org/10.1016/j.chom.2021.02.019

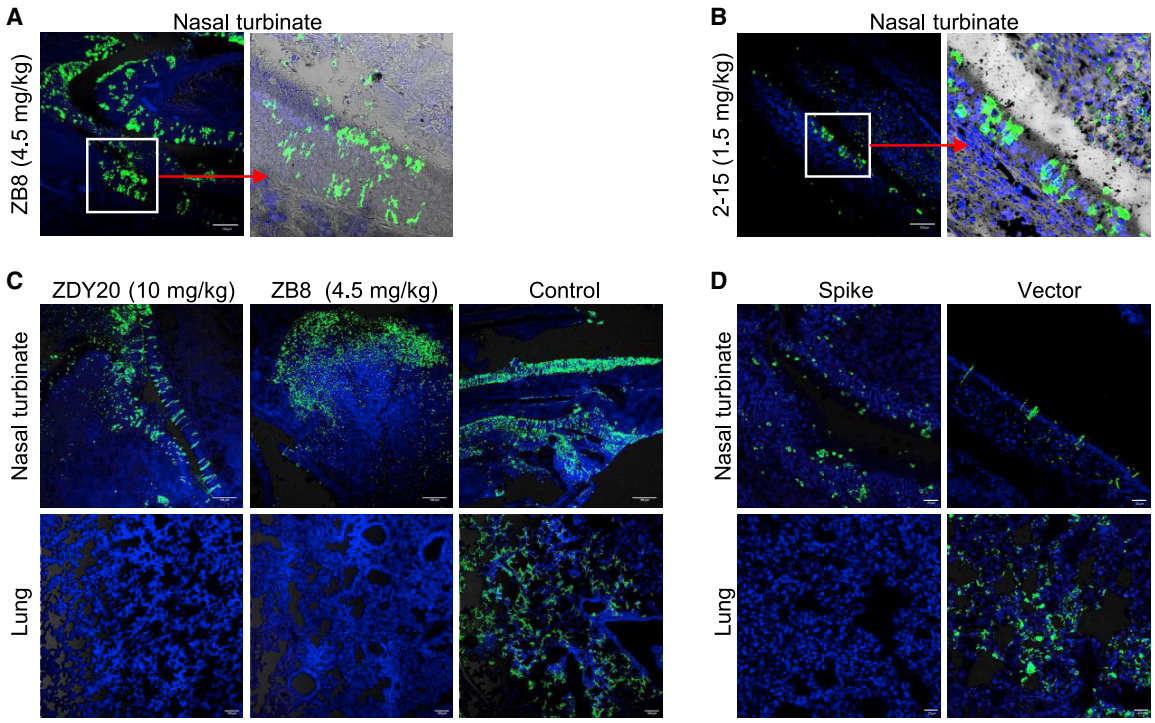

Figure 5. Robust SARS-CoV-2 infection in nasal turbinates at 4 dpi in the intraperitoneally injected HuNAb ZB8 and 2-15, intranasally administrated ZDY20 and ZB8, and DNA vaccine prophylaxis experiments

SARS-CoV-2 NP was stained green by IF staining, and cell nuclei were counterstained with DAPI (blue).

(A and B) Representative images of IF staining in nasal turbinates of hamsters intraperitoneally injected with 4.5 mg/kg ZB8 (A) and 1.5 mg/kg 2-15 (B), respectively, 24 h before the live virus challenge (Figures S5 and S6). The images of IF staining showed the abundancy and distribution of NP^+ cells at 50× magnification. The inset image was enlarged at 100× magnification to show that infected NP^+ cells can reach toward mucosal epithelial surface.

(C) Representative images of IF staining of hamster lung (bottom) and nasal turbinate (top) in the intranasal HuNAb prophylaxis experiment (Figure S7). The animals were intranasally administrated with 10 mg/kg ZDY20 and 4.5 mg/kg ZB8, respectively, 12 h before the live virus challenge. The images showed abundant and diffused distribution of NP^+ cells in the nasal turbinates but not in the lungs. Control animals showed diffused NP^+ expression in both nasal turbinates and lungs. Images were shown at the 50× magnification.

(D) Representative images of IF staining of hamster nasal turbinate (top) and lung (bottom) in the spike-based DNA vaccine experiment (Figure S8). The images of IF staining showed the abundancy and distribution of NP^+ cells in nasal turbinate but few in lung of a representative vaccinated hamster. The vector control hamster had abundant NP^+ cells both in nasal turbinate and lung. Images were shown at the 100× magnification.

See also Figures S4–S7 and Table S6.

These kinetics results demonstrated that earlier commencement of treatment within 2 dpi resulted in a more significant reduction of infectious viruses. For more significant viral load reduction, commencement of treatment within 1 dpi is likely necessary. To determine the role of ZDY20 in protection, we measured the antibody concentration and neutralization titer at 4 dpi. Over 40 μg/mL ZDY20 was found in 100% treated animals at 1 dpi, 75% treated animals at 2 dpi, and 50% treated animals at 3 dpi (Figure 6D; Table S5), together with mean IC_{50} values of 1:169, 1:62, and 1:69 in each corresponding group (Figure 6E), respectively.

Subsequently, we performed pathological analysis on lung specimens to understand whether ZDY20 protects against tissue injury in hamsters. The H&E-stained sections of control hamsters showed acute lung injury with peribronchiolar infiltration, bronchiolar epithelial cell death, diffuse alveolar wall thickening, patchy areas of alveolar space infiltration, exudation, and vasculitis (Figure 6F, top). In contrast, less severe histopathological changes were observed in all 3 groups of ZDY20-treated hamsters. There was no apparent peribronchiolar infiltration in hamsters treated at 1 dpi. The bronchiolar epithelia appeared normal, with only occasionally observed cell death in hamsters treated at 2 dpi. Moderate alveolar wall thickening and capillary congestion without alveolar space infiltration or exudation and limited vasculitis were observed in hamsters treated at 3 dpi. Corroboratively, abundant SARS-CoV-2 NP expression in the bronchiolar epithelium and alveoli was observed in the lungs of control hamsters (Figure 6F, bottom). In ZDY20-treated hamsters, NP expression was confined to small areas of alveoli at 1 dpi and was more frequently found in the bronchiolar epithelia at 2 and 3 dpi. The mean number of NP^+ cells per 50×field of lung tissues at 1 dpi was significantly lower than that of the control group (Figure 6G). Importantly, when we performed IF staining of viral NP antigen in nasal turbinate tissues, robust and diffuse viral NP expression in extensive areas lining the stratified squamous epithelia was found in infected hamsters treated with 10 mg/kg ZDY20 either at 1, 2, or 3 dpi, similar to untreated control hamsters (Figure 7A). These results demonstrated that postchallenge treatment with 10 mg/kg ZDY20 suppressed robust SARS-CoV-2 infection in the lungs but not in the nasal turbinates in

Please cite this article in press as: Zhou et al., Robust SARS-CoV-2 infection in nasal turbinates after treatment with systemic neutralizing antibodies, Cell Host & Microbe (2021), https://doi.org/10.1016/j.chom.2021.02.019

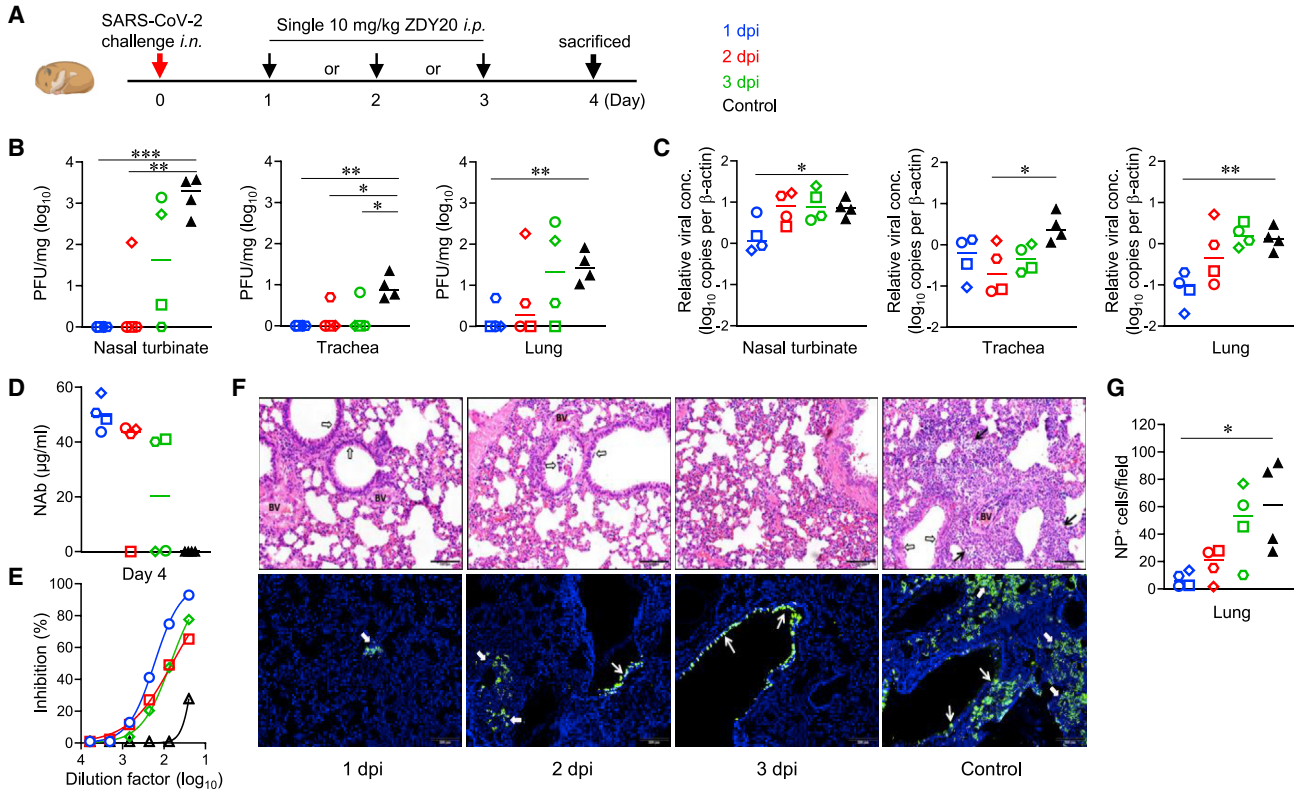

Figure 6. Postchallenge ZDY20 therapy suppresses SARS-CoV-2 replication in the lungs and acute lung injury

(A) Experimental schedule and color coding for each experimental group. After the live intranasal SARS-CoV-2 challenge, three groups of hamsters (n = 4 per group) received a single intraperitoneal injection of 10 mg/kg ZDY20 at 1, 2, or 3 dpi. The hamsters were sacrificed at 4 dpi for final analysis.

(B) A viral plaque assay was used to quantify infectious viruses in nasal turbinate, trachea, and lung tissue homogenates. Log_{10}-transformed PFUs per mg of tissue extractions were compared between treated hamsters at different time points and control animals.

(C) Sensitive RT-PCR was used to quantify the viral RNA copy numbers (normalized by β-actin) in nasal turbinate, trachea, and lung tissue homogenates.

(D and E) Serum concentration (D) and neutralizing activity (E) of HuNAb ZDY20 were determined by ELISA and pseudovirus assays, respectively.

(F) Representative images of hamster lung tissues by H&E (100×, top panel) and IF (50×, bottom panel). For the H&E staining results, the lungs of control hamsters showed peribronchiolar infiltration and bronchiolar epithelial cell death (open arrows), diffuse alveolar wall thickening, and patchy areas of alveolar space infiltration and exudation (arrows). One blood vessel in the middle of the section showed vasculitis (BV, blood vessel). For IF-stained viral NP antigen in the sections (50×), the lungs of control hamsters showed NP expression in bronchiolar epithelium (thin arrows) and diffuse NP expression in large areas of alveoli (thick arrows). SARS-CoV-2 NP was stained green, and cell nuclei were counterstained with DAPI (blue). In ZDY20-treated hamsters, NP expression was much confined to a small area of alveoli (thick arrows) or in the epithelia of bronchioles (thin arrows).

(G) NP^+ cells per 50×field were compared in the lungs of four experimental groups. Data of individual animals were indicated by different symbols, and different colors represented different groups. Statistics were generated using ordinary one-way ANOVA and multiple comparisons test. *$p < 0.05$; **$p < 0.01$; ***$p < 0.001$. See also Figures S4 and S9 and Table S5.

the hamster model (Figure 7B), suggesting the deficiency of systemic HuNAb to outcompete the viral replication within the nasal mucosal epithelia.

To further understand the difficulty of sterile protection in the URT, we sought to measure the amounts of intraperitoneally injected HuNAb in nasal wash and tissue homogenates. In contrast to high amounts of ZDY20, ZB8, and 2-15 detected in animal sera (Tables S5 and S6), no measurable amounts of antibodies were found in nasal wash specimens of hamsters tested. Various amounts of antibodies, however, were found in nasal turbinate and lung homogenates (Figure S9). When we included all hamsters from both ZDY20 prevention and treatment experiments together with 2-15 prevention (Figure S6) and intranasal prevention of ZDY20 and ZB8 (Figure S7) for analysis, the amount of peripheral HuNAb was negatively correlated with NP^+ cells in the lungs but not in the nasal turbinates (Figure 7C). Furthermore, there was a significant negative correlation between the tissue HuNAb concentration and the number of infectious viral PFUs either in nasal turbinate or in lung homogenates (except that nasal turbinates of five animals in the 2-15 prevention experiment were not available for measuring PFUs) (Figure 7D). Therefore, HuNAb in tissue homogenates might account for the significant reduction of infectious viral particles in both nasal turbinates and lungs once the antibody encounters the virus for neutralization during the PFU measurement experiment.

DISCUSSION

ZDY20, ZB8, and 2-15 represent the most promising class of RBD-specific HuNAbs that bind to the conformational

Please cite this article in press as: Zhou et al., Robust SARS-CoV-2 infection in nasal turbinates after treatment with systemic neutralizing antibodies, Cell Host & Microbe (2021), https://doi.org/10.1016/j.chom.2021.02.019

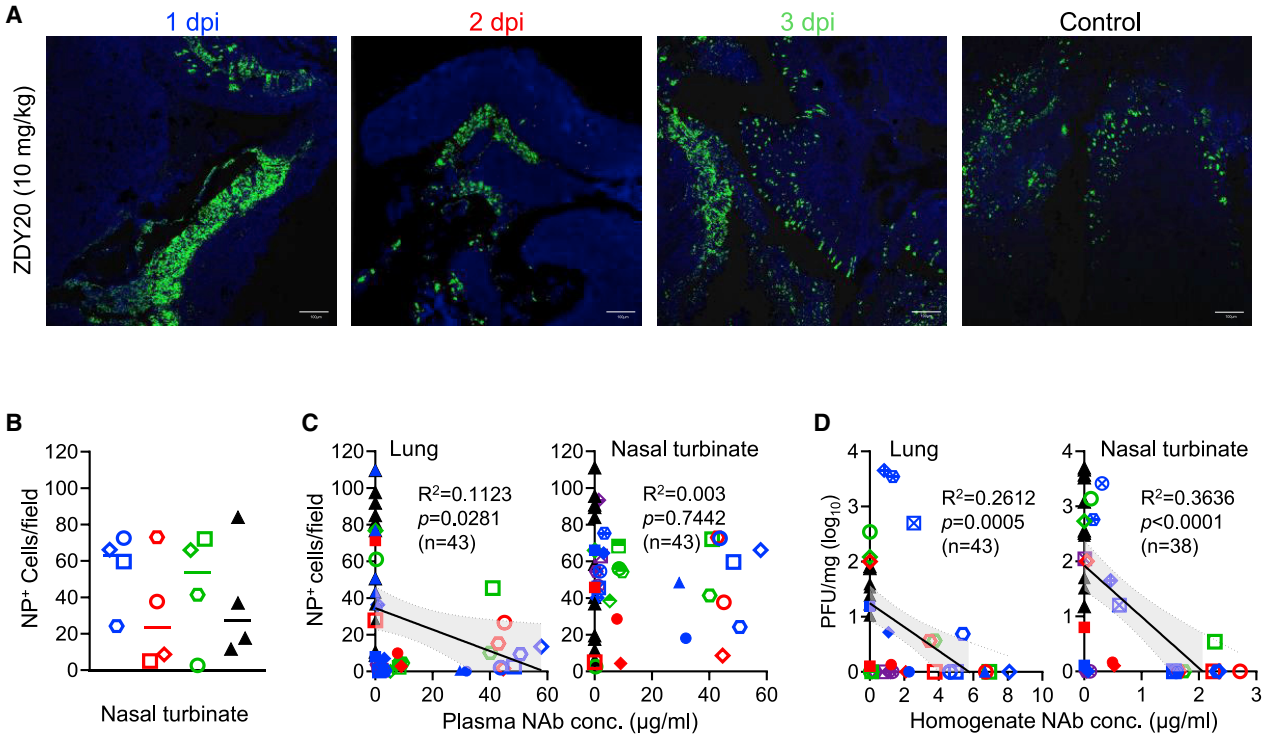

Figure 7. Postchallenge ZDY20 therapy does not suppress SARS-CoV-2 replication in nasal turbinates considerably by IF staining and correlation analysis

(A) Abundant numbers of NP^+ cells in nasal turbinates of hamsters treated at 1, 2, and 3 dpi compared with the untreated control animal. SARS-CoV-2 NP was stained green, and cell nuclei were counterstained with DAPI (blue). Images were shown at the 50× magnification.

(B) There were no significant differences among the nasal turbinates from four groups of experimental hamsters for NP^+ cells per 50×field.

(C) A negative correlation was found between NP^+ cells per 50×field in the lungs and the amount of peripheral ZDY20. No significant correlation was found between NP^+ cells per 50×field in nasal turbinates and the amount of peripheral ZDY20.

(D) There was a significant negative correlation between the tissue antibody concentration of ZDY20 and the number of infectious viral particles (PFUs) either in lung or in nasal turbinate homogenates. Correlation analyses were performed by linear regression using GraphPad Prism 6.0. Color-coded and different shapes of symbols were consistent with those in Figures 3 and 6.

See also Figures S4, S6, S7, and S9 and Tables S5 and S6.

determinants of the SARS-CoV-2 RBD overlapping with the cellular entry receptor ACE2 binding site (Cao et al., 2020; Liu et al., 2020b; Robbiani et al., 2020; Shi et al., 2020; Sun et al., 2020; Wu et al., 2020a, 2020b; Zost et al., 2020). Both SARS-CoV-2 and SARS-CoV use ACE2 to initiate infection, although they share only 40% amino acid identity in the RBD external subdomain (Chan et al., 2020b; Sahin et al., 2020; Wan et al., 2020; Zhou et al., 2020a). Structural analysis indicated that residues in the SARS-CoV-2 RBD that are essential for ACE2 binding are highly conserved or share similar side chain properties with those in the SARS-CoV RBD (Lan et al., 2020). During the natural course of infection, there was cross-reactivity between antibodies to SARS-CoV-2 and SARS-CoV, but only antibodies from COVID-19 patients neutralized SARS-CoV-2 (Wang et al., 2020b). Importantly, most SARS-CoV-2 HuNAbs primarily target distinct RBD epitopes overlapping with the ACE2 binding site (Cao et al., 2020; Liu et al., 2020b; Robbiani et al., 2020; Shi et al., 2020; Sun et al., 2020; Wu et al., 2020a; 2020b; Zost et al., 2020). This feature is critical because the ability of HuNAbs to compete with ACE2 for binding with the viral RBD often reflects their neutralizing potency. In particular, the potency of RBD-specific HuNAbs is stronger than those targeting the N-terminal domain (NTD) (Chi et al., 2020; Liu et al., 2020b; Rogers et al., 2020). These results corroborate our previous findings on SARS-CoV in that the RBD contains the major antigenic determinants for inducing potent NAbs (Chen et al., 2005; Yi et al., 2005). In this study, we consistently found that RBD-specific ZDY20 displayed neutralizing activity through competition for the ACE2 binding site. Our *in vivo* analysis of ZDY20, together with data of the two stronger RBD-specific ZB8 and 2-15, should have important implications for other HuNAbs that have similar functional properties and are now under clinical development (Cao et al., 2020; Liu et al., 2020b; Robbiani et al., 2020; Shi et al., 2020; Sun et al., 2020; Wu et al., 2020a, 2020b; Zost et al., 2020).

Protection of the URT through passive immunization of HuNAb or intramuscular vaccination is a very important issue of SARS-CoV-2 prevention and vaccine development (Krammer, 2020). Ciliated nasal epithelial cells in the URT have the highest ACE2 and transmembrane serine protease 2 (TMPRSS2) expression to support SARS-CoV-2 infection (Hou et al., 2020), which is consistent to our findings in SARS-CoV-2-infected hamsters (Chan et al., 2020a). Several potent RBD-specific HuNAbs have been evaluated for SARS-CoV-2 prevention in various

Please cite this article in press as: Zhou et al., Robust SARS-CoV-2 infection in nasal turbinates after treatment with systemic neutralizing antibodies, Cell Host & Microbe (2021), https://doi.org/10.1016/j.chom.2021.02.019

animal models (Liu et al., 2020b; Rogers et al., 2020; Shi et al., 2020; Zost et al., 2020). Most of these studies, however, have focused on viral load reduction in the lungs without detailed examination of viral replication in the URT tissues. In this study, we showed that systemic prophylaxis by ZDY20, ZB8, and 2-15 did not prevent SARS-CoV-2 infection significantly in nasal turbinate epithelia. In the presence of the prophylaxis, besides insignificantly suppressed viral loads, the large number of NP^+ cells at 4 dpi demonstrated robust SARS-CoV-2 infection in nasal turbinate tissues, although serum neutralization IC_{50} values were maintained over 1:200 at the time of virus challenge and over 1:50 at the time of animal sacrifice. We only observed significantly reduced numbers of infectious viruses (PFUs) in homogenized nasal turbinate tissues. We reasoned that the reduction was likely due to blood-derived potent HuNAb during tissue homogenization for the *in vitro* assay. Indeed, low amounts of ZDY20 and ZB8 were detected in homogenized nasal turbinate tissues. Moreover, the amount of HuNAb was negatively corelated with the PFU number of infectious viruses in both lung and nasal turbinate homogenates, suggesting that SARS-CoV-2 could be neutralized when it encountered the sufficient amount of neutralizing antibody. Since the amounts of ZDY20 and ZB8 were very low in nasal wash, our results suggested that the insufficient passive immunization for sterile protection is probably due to poor distribution of neutralizing antibodies on or within the viral entry portal of nasal turbinate to outcompete the robust viral infection there. This finding then brought the worry on vaccine-induced neutralizing antibodies for URT sterile protection. Based on experimental evidence, although the intramuscular DNA/electroporation vaccination induced high amounts of neutralizing antibodies, which were comparable to those of convalescent plasma or human vaccine recipients (Sadoff et al., 2021; Sahin et al., 2020; Xia et al., 2020), robust SARS-CoV-2 infection was still found in nasal turbinate tissues of experimentally infected hamsters. The subprotection may allow possibly HuNAb-resistant viruses to emerge. Collectively, these data highlight the need to explore vaccine-induced mucosal immunity (e.g., high amount of sIgA in URT) for the complete prevention of SARS-CoV-2 infection. Since COVID-19 patients have the highest viral load and viral shedding into saliva at or soon after presentation (To et al., 2020b), effective inhibition of SARS-CoV-2 replication in the URT would be critical for infection control. Mucosal protection faces a serious challenge because one-third of convalescent COVID-19 patients had serum IC_{50} values less than 1:50 (Robbiani et al., 2020), and therefore, they may be susceptible to reinfection. Indeed, we have recently documented the world's first reported case of SARS-CoV-2 reinfection in a Hong Kong patient whose serum NAb titer decreased from 1:40 to <1:10 within 140 days after an acute asymptomatic infection had virus shedding in the URT due to reinfection by another strain of SARS-CoV-2 (To et al., 2020a). Before we have an effective vaccine for sterile protection, our results strongly urge universal masking as the highest priority for SARS-CoV-2 prevention.

In our postchallenge treatment kinetics study, we showed that early use of ZDY20, preferably within 2 dpi, suppressed infectious virus, viral loads, and acute injury in the lungs of treated hamsters. In nasal turbinates, however, robust viral loads and NP^+ cells were readily observed for treatment even at 1 dpi, except for the reduced numbers of infectious viruses in homogenized tissues. Since the amount of peripheral ZDY20 was negatively correlated with NP^+ cells in the lungs but not in the nasal turbinates, the therapeutic efficacy of injected ZDY20 is likely limited in the URT. Several studies have evaluated the potency of RBD-specific HuNAbs for treating preinfected mice, hamsters, and monkeys (Baum et al., 2020; Cao et al., 2020; Shi et al., 2020; Wu et al., 2020b), but few have performed a treatment kinetics study. In hACE2-transgenic mice, a 20-mg/kg injection of BD-368-2 at 2 h post-infection (hpi) reduced the lung viral loads by approximately 3 logs (Cao et al., 2020). In another study, after a 25-mg/kg dose of a noncompeting pair of HuNAbs given at 12 hpi, viral loads were reduced for over 2 logs, yet there were still 10^6 copies/g of lung tissues at 3 days after virus challenge in hACE2-transgenic mice (Wu et al., 2020b). In monkey models, a preprint article indicated that SARS-CoV-2 viral loads were detected in nasopharyngeal swabs at 4 dpi in animals that received a very high dose of 150 mg/kg of the REGN-COV2 antibody cocktail at 1 dpi (Baum et al., 2020). Moreover, an intraperitoneal dose of 50 mg/kg treatment with the RBD-specific CB6 antibody that has an IC_{90} value of 1 μg/mL reduced but did not completely prevent histopathological changes in the lungs of SARS-CoV-2-infected monkeys (Shi et al., 2020). In addition to these HuNAb studies, for convalescent plasma therapy, we previously reported that convalescent sera of infected hamsters reduced SARS-CoV-2 replication but not acute lung injury (Chan et al., 2020a). Since the mortality rate of critically ill COVID-19 patients might be related to the IgG antibody levels in the transfused convalescent plasma (Joyner et al., 2020), it might be necessary to develop high-titer HuNAbs as specific antivirals for COVID-19 early treatment. In this study, by initiating ZDY20 treatment at the different time points of 1, 2, and 3 dpi, we demonstrated the benefits of commencing HuNAb treatment as early as possible in terms of better viral load reduction and alleviation of acute lung injury. Nevertheless, treatment started as late as 3 dpi still resulted in better histopathological changes in the lungs and therefore should still be considered in COVID-19 patients who presented later in the course of disease, as long as HuNAb did not promote acute lung injury (Liu et al., 2019).

In summary, we describe robust SARS-CoV-2 infection in nasal turbinates in the presence of potent systemic neutralizing antibodies in both prophylaxis and therapeutic studies in golden Syrian hamsters. Despite the presence of systemic serum HuNAb IgG, high viral loads and infected cells, as well as infectious viruses, may persist for at least 4 days in nasal turbinate tissues. Nevertheless, systemic ZDY20 is able to suppress SARS-CoV-2 replication and acute injury in the lungs of experimental hamsters. These findings have important implications for viral transmission, patient management, vaccine development, and control of reinfection.

Limitations of study

One limitation of study is that we could not determine the dose that RBD-specific HuNAb would be sufficient for sterile protection of the URT. Giving detectable viral loads in nasopharyngeal swabs at 4 dpi in monkeys that received a very high dose of 150 mg/kg of the REGN-COV2 antibody cocktail at 1 dpi (Baum et al., 2020), protection of the URT by IgG through systemic HuNAb or intramuscular vaccination can be quite difficult.

During our manuscript revision, Chen et al. published an RBD-specific HuNAb LY-CoV555 clinical study, examining three doses of 700, 2,800, and 7000-mg monotherapy (Chen et al., 2021). In this phase 2 trial, only the middle dose of LY-CoV555 appeared to accelerate the natural decline of viral loads in nasopharyngeal swaps over time, whereas the other doses had not by day 11. Systemic HuNAb is therefore unlikely sufficient to reach URT for immediate and complete viral suppression in humans, which is consistent with our findings in hamsters. For implications to vaccine development, three COVID-19 vaccines including the Pfizer-BioNTech BNT162B2 mRNA, the Moderna mRNA, and the Oxford-ChAdOx1 have released phase III trial results to support emergency use. Only the Oxford-ChAdOx1 vaccine has evaluated and indicated the low efficacy against asymptomatic infection (Voysey et al., 2021). In particular, the 3.8% efficacy among human vaccinees who received two standard doses was disappointing. Using the hamster model, our finding of robust viral replication in nasal turbinate outcompeting the vaccine-induced neutralizing antibodies has likely revealed a possible mechanism underlying the difficulty of the vaccine against asymptomatic infection. Another limitation of study is that we could not determine if viruses newly released from nasal turbinate tissues would be immediately neutralized by HuNAb because these viruses are difficult to separate from the inoculated viruses. The significantly reduced numbers of infectious viruses in homogenized nasal turbinate tissues measured by our plaque assay, however, provided evidence that viruses in the URT can be immediately neutralized when they encounter the HuNAb.

STAR★METHODS

Detailed methods are provided in the online version of this paper and include the following:

- KEY RESOURCES TABLE
- RESOURCE AVAILABILITY
  - Lead contact
  - Materials availability
  - Data and code availability
- EXPERIMENTAL MODEL AND SUBJECT DETAILS
  - Patients
  - Syrian hamsters
  - Cell lines
- METHOD DETAILS
  - Construction of a Fab Phage Display Library
  - Enrichment of antigen-binding clones by in-solution panning
  - Polyclonal, monoclonal phage and recombinant protein ELISAs
  - Protein expression, purification and Fab production
  - Pseudovirus-based neutralization assay
  - Neutralization activity of HuNAbs against live SARS-CoV-2
  - Antibody binding kinetics and competition with receptor ACE2 measured by SPR
  - Epitope mapping through a yeast surface display system
  - Syrian hamster experiments
  - DNA vaccination in Syrian hamsters
  - Histopathology and immunofluorescence (IF) staining
- QUANTIFICATION AND STATISTICAL ANALYSIS

SUPPLEMENTAL INFORMATION

Supplemental information can be found online at https://doi.org/10.1016/j.chom.2021.02.019.

ACKNOWLEDGMENTS

This study was partly supported by the Research Grants Council Collaborative Research Fund (C7156-20G to Z.C.); the University Development Fund and Li Ka Shing Faculty of Medicine Matching Fund from the University of Hong Kong to the AIDS Institute; the Innovation and Technology Fund, Innovation and Technology Commission, the Hong Kong Special Administrative Region Government; and the National Program on Key Research Project of China (grant nos. 2020YFA0707500 and 2020YFA0707504); and donations of the Friends of Hope Education Fund, the Shaw Foundation Hong Kong, Richard Yu and Carol Yu, Michael Seak-Kan Tong, May Tam Mak Mei Yin, Hui Ming, Lee Wan Keung Charity Foundation Limited, Hui Hoy and Chow Sin Lan Charity Fund Limited, Chan Yin Chuen Memorial Charitable Foundation, Marina Man-Wai Lee, the Hong Kong Hainan Commercial Association South China Microbiology Research Fund, the Jessie & George Ho Charitable Foundation, Perfect Shape Medical Limited, Kai Chong Tong, Foo Oi Foundation Limited, Tse Kam Ming Laurence, Betty Hing-Chu Lee, Ping Cham So, and Lo Ying Shek Chi Wai Foundation. Z.C.'s team was also partly supported by the Theme-Based Research Scheme (T11-706/18-N to Z.C.). The funding sources had no role in the study design, data collection, analysis, interpretation, or writing of the report. We thank Yik-Chun Wong for partial DNA vaccine experiment. We also thank Zack Saud for generously sharing his optimized phage display protocols and guidance on the panning procedures.

AUTHOR CONTRIBUTIONS

Z.C. and K.-Y.Y. supervised two collaborative teams in the study. D.Z., B.Z., J.F.-W.C., R.Z., and Z.C. designed the experiments, analyzed the data, and wrote the manuscript. D.Z. generated four ZDY HuNAbs. B.Z. generated ZB8. D.D.H. provided 2-15. J.F.iW.C., R.Z., C.C.-S.C., V.K.-M.P., S.Y., H.X., K.K.-H.C., C.C.-Y.C., and J.C. conducted hamster, viral load, and live virus experiments. R.Z. and K.K.-W.T. prepared and studied clinical samples. K.-Y.K., Z.D., and T.T.-K.L. performed the immunofluorescence staining of the hamster tissue section. L.L. and A.J.Z. analyzed tissue pathology. S.L. performed yeast spike display and antibody epitope mapping. S.J.C., B.Z., and C.-Y.C. conducted antibody experiments. S.S., Q.Z., and LZ performed the Biocore analysis on HuNAbs. C.L. and J.Z. performed live virus neutralization.

DECLARATION OF INTERESTS

J.F.-W.C. has received travel grants from Pfizer Corporation Hong Kong and Astellas Pharma Hong Kong Corporation Limited and was an invited speaker for Gilead Sciences Hong Kong Limited and Luminex Corporation. The other authors declare no conflicts of interest except for a provisional patent application filed for human monoclonal antibodies generated in our laboratory by the University of Hong Kong. The funding sources had no role in study design, data collection, analysis, interpretation, or writing of the report.

Received: December 21, 2020
Revised: February 1, 2021
Accepted: February 19, 2021
Published: February 25, 2021

REFERENCES

Baum, A., Ajithdoss, D., Copin, R., Zhou, A., Lanza, K., Negron, N., Ni, M., Wei, Y., Mohammadi, K., Musser, B., et al. (2020). REGN-COV2 antibodies prevent and treat SARS-CoV-2 infection in rhesus macaques and hamsters. Science *370*, 1110–1115.

Boulware, D.R., Pullen, M.F., Bangdiwala, A.S., Pastick, K.A., Lofgren, S.M., Okafor, E.C., Skipper, C.P., Nascene, A.A., Nicol, M.R., Abassi, M., et al. (2020). A Randomized Trial of Hydroxychloroquine as Postexposure Prophylaxis for Covid-19. N. Engl. J. Med. *383*, 517–525.

Cao, Y., Su, B., Guo, X., Sun, W., Deng, Y., Bao, L., Zhu, Q., Zhang, X., Zheng, Y., Geng, C., et al. (2020). Potent Neutralizing Antibodies against SARS-CoV-2 Identified by High-Throughput Single-Cell Sequencing of Convalescent Patients' B Cells. Cell *182*, 73–84.e16.

Chames, J.M.P. (2012). Phage display and selections on purified antigens. In Antibody Engineering: Methods and Protocols, Second Edition, P. Chames, ed. (Humana Press Inc.), pp. 213–224.

Chan, J.F.-W., Zhang, A.J., Yuan, S., Poon, V.K.-M., Chan, C.C.-S., Lee, A.C.-Y., Chan, W.-M., Fan, Z., Tsoi, H.-W., Wen, L., et al. (2020a). Simulation of the clinical and pathological manifestations of Coronavirus Disease 2019 (COVID-19) in golden Syrian hamster model: implications for disease pathogenesis and transmissibility. Clinical Infectious Diseases *71*, 2428–2446.

Chan, J.F., Kok, K.H., Zhu, Z., Chu, H., To, K.K., Yuan, S., and Yuen, K.Y. (2020b). Genomic characterization of the 2019 novel human-pathogenic coronavirus isolated from a patient with atypical pneumonia after visiting Wuhan. Emerg. Microbes Infect. *9*, 221–236.

Chan, J.F., Yip, C.C., To, K.K., Tang, T.H., Wong, S.C., Leung, K.H., Fung, A.Y., Ng, A.C., Zou, Z., Tsoi, H.W., et al. (2020c). Improved Molecular Diagnosis of COVID-19 by the Novel, Highly Sensitive and Specific COVID-19-RdRp/Hel Real-Time Reverse Transcription-PCR Assay Validated *In Vitro* and with Clinical Specimens. J. Clin. Microbiol. *58*, 00310–00320.

Chan, J.F., Yuan, S., Kok, K.H., To, K.K., Chu, H., Yang, J., Xing, F., Liu, J., Yip, C.C., Poon, R.W., et al. (2020d). A familial cluster of pneumonia associated with the 2019 novel coronavirus indicating person-to-person transmission: a study of a family cluster. Lancet *395*, 514–523.

Chao, G., Lau, W.L., Hackel, B.J., Sazinsky, S.L., Lippow, S.M., and Wittrup, K.D. (2006). Isolating and engineering human antibodies using yeast surface display. Nat. Protoc. *1*, 755–768.

Chen, Z., Zhang, L., Qin, C., Ba, L., Yi, C.E., Zhang, F., Wei, Q., He, T., Yu, W., Yu, J., et al. (2005). Recombinant modified vaccinia virus Ankara expressing the spike glycoprotein of severe acute respiratory syndrome coronavirus induces protective neutralizing antibodies primarily targeting the receptor binding region. J. Virol. *79*, 2678–2688.

Chen, P., Nirula, A., Heller, B., Gottlieb, R.L., Boscia, J., Morris, J., Huhn, G., Cardona, J., Mocherla, B., Stosor, V., et al.; BLAZE-1 Investigators (2021). SARS-CoV-2 Neutralizing Antibody LY-CoV555 in Outpatients with Covid-19. N. Engl. J. Med. *384*, 229–237.

Chi, X., Yan, R., Zhang, J., Zhang, G., Zhang, Y., Hao, M., Zhang, Z., Fan, P., Dong, Y., Yang, Y., et al. (2020). A neutralizing human antibody binds to the N-terminal domain of the Spike protein of SARS-CoV-2. Science *369*, 650–655.

Chu, H., Chan, J.F.-W., Yuen, T.T.-T., Shuai, H., Yuan, S., Wang, Y., Hu, B., Yip, C.C.-Y., Tsang, J.O.-L., Huang, X., et al. (2020). Comparative tropism, replication kinetics, and cell damage profiling of SARS-CoV-2 and SARS-CoV with implications for clinical manifestations, transmissibility, and laboratory studies of COVID-19: an observational study. The Lancet Microbe *1*, e14–e23.

Dalamaga, M., Karampela, I., and Mantzoros, C.S. (2020). Commentary: Could iron chelators prove to be useful as an adjunct to COVID-19 Treatment Regimens? Metabolism *108*, 154260.

Duan, K., Liu, B., Li, C., Zhang, H., Yu, T., Qu, J., Zhou, M., Chen, L., Meng, S., Hu, Y., et al. (2020). Effectiveness of convalescent plasma therapy in severe COVID-19 patients. Proc. Natl. Acad. Sci. USA *117*, 9490–9496.

Goldman, J.D., Lye, D.C.B., Hui, D.S., Marks, K.M., Bruno, R., Montejano, R., Spinner, C.D., Galli, M., Ahn, M.Y., Nahass, R.G., et al.; GS-US-540-5773 Investigators (2020). Remdesivir for 5 or 10 Days in Patients with Severe Covid-19. N. Engl. J. Med. *383*, 1827–1837.

Guo, J., Zuo, T., Cheng, L., Wu, X., Tang, J., Sun, C., Feng, L., Chen, L., Zhang, L., and Chen, Z. (2015). Simian immunodeficiency virus infection evades vaccine-elicited antibody responses to V2 region. J. Acquir. Immune Defic. Syndr. *68*, 502–510.

Hou, Y.J., Okuda, K., Edwards, C.E., Martinez, D.R., Asakura, T., Dinnon, K.H., 3rd, Kato, T., Lee, R.E., Yount, B.L., Mascenik, T.M., et al. (2020). SARS-CoV-2 Reverse Genetics Reveals a Variable Infection Gradient in the Respiratory Tract. Cell *182*, 429–446.14.

Hung, I.F., Cheng, V.C., Li, X., Tam, A.R., Hung, D.L., Chiu, K.H., Yip, C.C., Cai, J.P., Ho, D.T., Wong, S.C., et al. (2020a). SARS-CoV-2 shedding and seroconversion among passengers quarantined after disembarking a cruise ship: a case series. Lancet Infect. Dis. *20*, 1051–1060.

Hung, I.F., Lung, K.C., Tso, E.Y., Liu, R., Chung, T.W., Chu, M.Y., Ng, Y.Y., Lo, J., Chan, J., Tam, A.R., et al. (2020b). Triple combination of interferon beta-1b, lopinavir-ritonavir, and ribavirin in the treatment of patients admitted to hospital with COVID-19: an open-label, randomised, phase 2 trial. Lancet *395*, 1695–1704.

Jiang, H.W., Li, Y., Zhang, H.N., Wang, W., Yang, X., Qi, H., Li, H., Men, D., Zhou, J., and Tao, S.C. (2020). SARS-CoV-2 proteome microarray for global profiling of COVID-19 specific IgG and IgM responses. Nat. Commun. *11*, 3581.

Joyner, M.J., Senefeld, J.W., Klassen, S.A., Mills, J.R., Johnson, P.W., Theel, E.S., Wiggins, C.C., Bruno, K.A., Klompas, A.M., Lesser, E.R., et al. (2020). Effect of Convalescent Plasma on Mortality among Hospitalized Patients with COVID-19: Initial Three-Month Experience. medRxiv. https://doi.org/10.1101/2020.08.12.20169359.

Krammer, F. (2020). SARS-CoV-2 vaccines in development. Nature *586*, 516–527.

Lan, J., Ge, J., Yu, J., Shan, S., Zhou, H., Fan, S., Zhang, Q., Shi, X., Wang, Q., Zhang, L., and Wang, X. (2020). Structure of the SARS-CoV-2 spike receptor-binding domain bound to the ACE2 receptor. Nature *581*, 215–220.

Liu, L., Wei, Q., Lin, Q., Fang, J., Wang, H., Kwok, H., Tang, H., Nishiura, K., Peng, J., Tan, Z., et al. (2019). Anti-spike IgG causes severe acute lung injury by skewing macrophage responses during acute SARS-CoV infection. JCI Insight *4*, e123158.

Liu, L., To, K.K.-W., Chan, K.-H., Wong, Y.-C., Zhou, R., Kwan, K.-Y., Fong, C.H.-Y., Chen, L.-L., Choi, C.Y.-K., Lu, L., et al. (2020a). High neutralizing antibody titer in intensive care unit patients with COVID-19. Emerg. Microbes Infect. *9*, 1664–1670.

Liu, L., Wang, P., Nair, M.S., Yu, J., Rapp, M., Wang, Q., Luo, Y., Chan, J.F., Sahi, V., Figueroa, A., et al. (2020b). Potent neutralizing antibodies against multiple epitopes on SARS-CoV-2 spike. Nature *584*, 450–456.

Liu, P., Cai, J., Jia, R., Xia, S., Wang, X., Cao, L., Zeng, M., and Xu, J. (2020c). Dynamic surveillance of SARS-CoV-2 shedding and neutralizing antibody in children with COVID-19. Emerg. Microbes Infect. *9*, 1254–1258.

Hust, M., Frenzel, A., Meyer, T., Schirrmann, T., and Dübel, S. (2012). Construction of human naive antibody gene libraries. Methods Mol. Biol. *907*, 85–107.

Peiris, J.S., Chu, C.M., Cheng, V.C., Chan, K.S., Hung, I.F., Poon, L.L., Law, K.I., Tang, B.S., Hon, T.Y., Chan, C.S., et al.; HKU/UCH SARS Study Group (2003). Clinical progression and viral load in a community outbreak of coronavirus-associated SARS pneumonia: a prospective study. Lancet *361*, 1767–1772.

Riva, L., Yuan, S., Yin, X., Martin-Sancho, L., Matsunaga, N., Pache, L., Burgstaller-Muehlbacher, S., De Jesus, P.D., Teriete, P., Hull, M.V., et al. (2020). Discovery of SARS-CoV-2 antiviral drugs through large-scale compound repurposing. Nature *586*, 113–119.

Robbiani, D.F., Gaebler, C., Muecksch, F., Lorenzi, J.C.C., Wang, Z., Cho, A., Agudelo, M., Barnes, C.O., Gazumyan, A., Finkin, S., et al. (2020). Convergent antibody responses to SARS-CoV-2 in convalescent individuals. Nature *584*, 437–442.

Rogers, T.F., Zhao, F., Huang, D., Beutler, N., Burns, A., He, W.T., Limbo, O., Smith, C., Song, G., Woehl, J., et al. (2020). Isolation of potent SARS-CoV-2 neutralizing antibodies and protection from disease in a small animal model. Science *369*, 956–963.

Sadoff, J., Le Gars, M., Shukarev, G., Heerwegh, D., Truyers, C., de Groot, A.M., Stoop, J., Tete, S., Van Damme, W., Leroux-Roels, I., et al. (2021). Interim Results of a Phase 1-2a Trial of Ad26.COV2.S Covid-19 Vaccine. N. Engl. J. Med. https://doi.org/10.1056/NEJMoa2034201.

Sahin, U., Muik, A., Derhovanessian, E., Vogler, I., Kranz, L.M., Vormehr, M., Baum, A., Pascal, K., Quandt, J., Maurus, D., et al. (2020). COVID-19 vaccine BNT162b1 elicits human antibody and T_H1 T cell responses. Nature *586*, 594–599.

Shi, R., Shan, C., Duan, X., Chen, Z., Liu, P., Song, J., Song, T., Bi, X., Han, C., Wu, L., et al. (2020). A human neutralizing antibody targets the receptor-binding site of SARS-CoV-2. Nature *584*, 120–124.

Sun, Z., Chen, C., Li, W., Martinez, D.R., Drelich, A., Baek, D.S., Liu, X., Mellors, J.W., Tseng, C.T., Baric, R.S., and Dimitrov, D.S. (2020). Potent neutralization of SARS-CoV-2 by human antibody heavy-chain variable domains isolated from a large library with a new stable scaffold. MAbs *12*, 1778435.

Suthar, M.S., Zimmerman, M.G., Kauffman, R.C., Mantus, G., Linderman, S.L., Hudson, W.H., Vanderheiden, A., Nyhoff, L., Davis, C.W., Adekunle, O., et al. (2020). Rapid Generation of Neutralizing Antibody Responses in COVID-19 Patients. Cell Rep. Med. *1*, 100040.

Tan, W., Lu, Y., Zhang, J., Wang, J., Dan, Y., Tan, Z., He, X., Qian, C., Sun, Q., Hu, Q., et al. (2020). Viral Kinetics and Antibody Responses in Patients with COVID-19. medRxiv. https://doi.org/10.1101/2020.03.24.20042382.

To, K.K., Hung, I.F., Ip, J.D., Chu, A.W., Chan, W.M., Tam, A.R., Fong, C.H., Yuan, S., Tsoi, H.W., Ng, A.C., et al. (2020a). Coronavirus Disease 2019 (COVID-19) Re-infection by a Phylogenetically Distinct Severe Acute Respiratory Syndrome Coronavirus 2 Strain Confirmed by Whole Genome Sequencing. Clin. Infect. Dis. https://doi.org/10.1093/cid/ciaa1275.

To, K.K., Tsang, O.T., Leung, W.S., Tam, A.R., Wu, T.C., Lung, D.C., Yip, C.C., Cai, J.P., Chan, J.M., Chik, T.S., et al. (2020b). Temporal profiles of viral load in posterior oropharyngeal saliva samples and serum antibody responses during infection by SARS-CoV-2: an observational cohort study. Lancet Infect. Dis. *20*, 565–574.

Voysey, M., Clemens, S.A.C., Madhi, S.A., Weckx, L.Y., Folegatti, P.M., Aley, P.K., Angus, B., Baillie, V.L., Barnabas, S.L., Bhorat, Q.E., et al.; Oxford COVID Vaccine Trial Group (2021). Safety and efficacy of the ChAdOx1 nCoV-19 vaccine (AZD1222) against SARS-CoV-2: an interim analysis of four randomised controlled trials in Brazil, South Africa, and the UK. Lancet *397*, 99–111.

Wan, Y., Shang, J., Graham, R., Baric, R.S., and Li, F. (2020). Receptor Recognition by the Novel Coronavirus from Wuhan: an Analysis Based on Decade-Long Structural Studies of SARS Coronavirus. J. Virol. *94*, 00120–00127.

Wang, P., Liu, L., Nair, M.S., Yin, M.T., Luo, Y., Wang, Q., Yuan, T., Mori, K., Solis, A.G., Yamashita, M., et al. (2020a). SARS-CoV-2 neutralizing antibody responses are more robust in patients with severe disease. Emerg. Microbes Infect. *9*, 2091–2093.

Wang, Y., Zhang, L., Sang, L., Ye, F., Ruan, S., Zhong, B., Song, T., Alshukairi, A.N., Chen, R., Zhang, Z., et al. (2020b). Kinetics of viral load and antibody response in relation to COVID-19 severity. J. Clin. Invest. *130*, 5235–5244.

Wu, Y., Li, C., Xia, S., Tian, X., Kong, Y., Wang, Z., Gu, C., Zhang, R., Tu, C., Xie, Y., et al. (2020a). Identification of Human Single-Domain Antibodies against SARS-CoV-2. Cell Host Microbe *27*, 891–898.e5.

Wu, Y., Wang, F., Shen, C., Peng, W., Li, D., Zhao, C., Li, Z., Li, S., Bi, Y., Yang, Y., et al. (2020b). A noncompeting pair of human neutralizing antibodies block COVID-19 virus binding to its receptor ACE2. Science *368*, 1274–1278.

Xia, S., Duan, K., Zhang, Y., Zhao, D., Zhang, H., Xie, Z., Li, X., Peng, C., Zhang, Y., Zhang, W., et al. (2020). Effect of an Inactivated Vaccine Against SARS-CoV-2 on Safety and Immunogenicity Outcomes: Interim Analysis of 2 Randomized Clinical Trials. JAMA *324*, 951–960.

Yi, C.E., Ba, L., Zhang, L., Ho, D.D., and Chen, Z. (2005). Single amino acid substitutions in the severe acute respiratory syndrome coronavirus spike glycoprotein determine viral entry and immunogenicity of a major neutralizing domain. J. Virol. *79*, 11638–11646.

Yuan, M., Liu, H., Wu, N.C., Lee, C.-C.D., Zhu, X., Zhao, F., Huang, D., Yu, W., Hua, Y., Tien, H., et al. (2020). Structural basis of a shared antibody response to SARS-CoV-2. Science *369*, 1119–1123.

Zhou, R., To, K.K., Wong, Y.C., Liu, L., Zhou, B., Li, X., Huang, H., Mo, Y., Luk, T.Y., Lau, T.T., et al. (2020b). Acute SARS-CoV-2 infection impairs dendritic cell and T cell responses. Immunity *53*, 864–877.e5.

Zhou, P., Yang, X.L., Wang, X.G., Hu, B., Zhang, L., Zhang, W., Si, H.R., Zhu, Y., Li, B., Huang, C.L., et al. (2020). A pneumonia outbreak associated with a new coronavirus of probable bat origin. Nature *579*, 270–273.

Zhu, N., Zhang, D., Wang, W., Li, X., Yang, B., Song, J., Zhao, X., Huang, B., Shi, W., Lu, R., et al.; China Novel Coronavirus Investigating and Research Team (2020). A Novel Coronavirus from Patients with Pneumonia in China, 2019. N. Engl. J. Med. *382*, 727–733.

Zost, S.J., Gilchuk, P., Case, J.B., Binshtein, E., Chen, R.E., Nkolola, J.P., Schäfer, A., Reidy, J.X., Trivette, A., Nargi, R.S., et al. (2020). Potently neutralizing and protective human antibodies against SARS-CoV-2. Nature *584*, 443–449.

Zuo, T., Shi, X., Liu, Z., Guo, L., Zhao, Q., Guan, T., Pan, X., Jia, N., Cao, W., Zhou, B., et al. (2011). Comprehensive analysis of pathogen-specific antibody response in vivo based on an antigen library displayed on surface of yeast. J. Biol. Chem. *286*, 33511–33519.

Please cite this article in press as: Zhou et al., Robust SARS-CoV-2 infection in nasal turbinates after treatment with systemic neutralizing antibodies, Cell Host & Microbe (2021), https://doi.org/10.1016/j.chom.2021.02.019

STAR★METHODS

KEY RESOURCES TABLE

REAGENT or RESOURCE	SOURCE	IDENTIFIER
Antibodies		
AF488 goat anti-rabbit IgG (H+L)	Life Technologies	Cat# A11034; RRID: AB_ 2576217
AF546 goat anti-human IgG (H+L)	Invitrogen	Cat# A21089; RRID: AB_ 2535745
FITC-conjugated donkey anti-rabbit IgG	Jackson ImmunoResearch	Cat# 711-095-152; RRID: AB_2315776
rabbit anti-SARS-CoV-2-N protein	Sino Biological	Cat# 40143-R019; RRID: AB_2827973
Hoechst 33258, Pentahydrate (bis-Benzimide)	Molecular Probes	Cat# H3569; RRID: AB_2651133
Bacterial and virus srains		
TG1 Electrocompetent Cells	Lucigen	Cat# 60502-1
M13KO7 Helper Phage	New England BioLabs	Cat# N0315S
SARS-CoV-2	HKU-001a strain	GenBank accession no: MT230904.1
Biological samples		
Blood sample from COVID-19 patients	Queen Mary Hospital	N/A
Chemicals, peptides, and recombinant proteins		
Biotinylated SARS-CoV-2 spike protein RBD	ACROBiosystems	Cat# SPD-C82E9-200ug
ACE2 protein	ACROBiosystems	Cat# AC2-H52H8-1mg
SARS-CoV-2 spike protein	ACROBiosystems	Cat# SPN-C52H8-500ug
Recombinant Protein G Agarose	Thermo Fisher Scientific	Cat# 15920010
Trimethylamine (TEA)	Sigma-Aldrich	Cat# 471283-500ML
HEPES buffer (1M)	GIBCO	Cat# 15630080
Anti-M13 Major Coat Protein Antibody-HRP	Santa Cruz Biotechnology	Cat# sc-53004 HRP
Goat anti-Human IgG Cross-Adsorbed Secondary Antibody, HRP	Invitrogen	Cat# 62-8420
3, 3¢,5, 5¢-Tetramethylbenzidine Liquid Substrate	Sigma-Aldrich T4444	Cat# T4444
Antigen Unmasking Solution (Citrate-Based)	Vector Laboratories	Cat# H3300; RRID: AB_2336226
Protease Lys-C	Roche	Cat# 11047825001
Protein A Sepharose	GenScript	Cat# L00210-50
Critical commercial assays		
RNeasy Mini Kit	QIAGEN	Cat# 74106
PrimeScript™ 1st strand cDNA Synthesis Kit	TaKaRa	Cat# 6210B
NEBuilder® HiFi DNA Assembly Master Mix	New England BioLabs	Cat# E2621L
Luciferase Assay System	Promega	Cat# E1501
Experimental models: cell lines		
HEK293T-hACE2 cells	In house	N/A
Vero-E6 cells	ATCC	Cat# CRL-1586
Expi293F™ Cells	Thermo Fisher Scientific	Cat# A14527; RRID: CVCL_D615
Experimental models: organisms/strains		
Golden Syrian hamster	Chinese University of Hong Kong Laboratory Animal Service Center	N/A

(*Continued on next page*)

Continued

REAGENT or RESOURCE	SOURCE	IDENTIFIER
Oligonucleotides		
	Table S7	N/A
Recombinant DNA		
AbVec2.0-IGHG1 plasmid	Addgene	Cat# 80795; RRID: Addgene_80795
AbVec1.1-IGKC plasmid	Addgene	Cat# 80796; RRID: Addgene_80796
pVAX1 vector	Invitrogen	Cat# V26020
pComb3X plasmid	Addgene	Cat# 63891; RRID: Addgene_63891
Software and algorithms		
Biacore Insight Evaluation software	GE Healthcare	RRID: SCR_015936
GraphPad Prism 6	https://www.graphpad.com/scientific-software/prism/	RRID: SCR_002798
Sequencher 5.4.6.	Gene Codes Corporation	RRID: SCR_001528
ImageJ	https://imagej.nih.gov/ij/download.html	RRID: SCR_003070

RESOURCE AVAILABILITY

Lead contact

Further information and requests for resources and reagents should be directed to and will be fulfilled by the Lead Contact, Zhiwei Chen (zchenai@hku.hk).

Materials availability

This study did not generate new unique reagents.

Data and code availability

The study did not generate any unique datasets or codes.

EXPERIMENTAL MODEL AND SUBJECT DETAILS

Patients

A total of 12 patients with COVID-19 were recruited between February and March 2020. All patient cases were confirmed by reverse-transcription polymerase chain reaction (RT-PCR) as described previously (Chan et al., 2020c). Clinical and laboratory findings were entered into a predesigned database. Written informed consent was obtained from all patients. This study was approved by the Institutional Review Board of the University of Hong Kong/Hospital Authority Hong Kong West Cluster, Hong Kong East Cluster Research Ethics Committee, and Kowloon West Cluster Research Ethics Committee (UW 13-265, HKECREC-2018-068, KW/EX-20-038[144-26]).

Syrian hamsters

Animal experimental plan was approved by the Committee on the Use of Live Animals in Teaching and Research (CULATR 5359-20) of the University of Hong Kong (HKU). Male and female Syrian hamsters (aged 6–10 weeks) were purchased from the Chinese University of Hong Kong Laboratory Animal Service Centre through the HKU Laboratory Animal Unit (LAU). The animals were kept in Biosafety Level-2 housing and given access to standard pellet feed and water *ad libitum* following LAU's standard operational procedures (SOPs). The viral challenge experiments were then conducted in our Biosafety Level-3 animal facility following SOPs strictly.

Cell lines

HEK293T-hACE2 and Vero E6 cells were maintained in Dulbecco's Modified Eagle Medium (DMEM) (Thermo Fisher Scientific) containing 10% Fetal bovine serum, 2 mM L-glutamine and 100 U/mL penicillin and were incubated at 37°C in 5% CO2 setting (Liu et al., 2019). Expi293F™ cells were maintained in Expi293™ Expression Medium (Thermo Fisher Scientific) and were incubated in a 37°C incubator with ^{3}80% relative humidity and 5% CO2 setting on an orbital shaker platform at 125 ± 5 rpm (New Brunswick innova™ 2100) according to the manufacturer's instructions.

METHOD DETAILS

Construction of a Fab Phage Display Library

Total RNA was extracted from peripheral blood lymphocytes of convalescent SARS-CoV2 patients by RNeasy Mini kit (QIAGEN), and both total RNA and mRNA were reverse transcribed into cDNA using PrimeScript 1st strand cDNA Synthesis Kit (Takara). Fd segment

Please cite this article in press as: Zhou et al., Robust SARS-CoV-2 infection in nasal turbinates after treatment with systemic neutralizing antibodies, Cell Host & Microbe (2021), https://doi.org/10.1016/j.chom.2021.02.019

(variable and first constant domain of the heavy chain genes and light-chain genes) were amplified by using primers (Table S7) specific for the human chain genes (Hust et al., 2012). Then, the amplified chains were assembled into the pComb3X phage display vector using the NEBuilder® HiFi DNA Assembly Cloning Kit (New England BioLabs, NEB). The assembled products were transformed into *Escherichia coli* TG1 (Lucigen) and resulted in a library of 3×10^6 clones. The transformants were expanded into a volume of 2 L, and the resulting phage was recovered as described previously (Hust et al., 2012).

Enrichment of antigen-binding clones by in-solution panning

This panning procedure was adapted from previously described procedures (Chames, 2012). For the first round of panning, 100 μl streptavidin magnetic beads (Thermo Fisher Scientific) were coated with 200 nM biotinylated SARS-CoV-2 spike protein RBD (ACROBiosystems), which were then blocked with 2% skimmed milk PBS for an h. At the same time, 1×10^{12} phages from the Fab phage library were also blocked in 2% skimmed milk PBS. Then, the mixture of phage and biotinylated RBD on beads was incubated for an h at room temperature (RT) on a rotating wheel. Then, the beads were pulled out of solution and washed 5 times with 1 mL of PBS Tween 20 (0.1%) and 2 times with 1 mL of PBS. The remaining phage was eluted with 0.1 M trimethylamine (TEA) and 0.2 M glycine pH 2 sequentially and then immediately neutralized with 1 M Tris base. The eluted phage was amplified by infection of *Escherichia coli* TG1 cultures, which were followed by superinfection with helper phage M13KO7 (NEB). At Round 2, 100 nM antigen was used with 50 μl beads. Then, 25 washes were performed at Round 2 to narrow down the Round 1 phage output to enrich for those that bind specifically to the target. Similarly, at Round 3, 25 washes were performed to narrow down the diversity and enrich for only specific, stronger binders from the phage library. Polyclonal phage ELISA was carried out at Round 2, and if phages were not sufficiently enriched at this stage, then a third round was carried out. All panning procedures were performed in solution using low protein binding 1.5 mL Eppendorf tubes.

Polyclonal, monoclonal phage and recombinant protein ELISAs

The procedures of phage ELISA were adapted from previously described procedures (Chames, 2012). For polyclonal phage ELISA, the RBD proteins were coated on 96-well enzyme-linked immunosorbent assay plates at 50 ng/well. After blocking with 4% skimmed milk in PBS, 50 μL phage library or amplified eluted phage was added to the plates at serial dilutions starting from 1:5 and then incubated for 1 h at room temperature. The plates were washed, and the anti-M13 Major Coat Protein Antibody-HRP (Santa Cruz Biotechnology) was added prior to color development by 3,3¢,5,5¢-Tetramethylbenzidine liquid substrate (Sigma-Aldrich). Optical density at 450 nm was read on a Varioskan LUX multimode microplate reader (Thermo Fisher Scientific). For monoclonal phage ELISA, a single colony was picked from the plate of eluted phage and cultured in 96-deep-well plates with approximately 200 μl/well at 37°C and 250 rpm. When the OD600 reached 0.5, each well of the single colony culture was superinfected with helper phage M13KO7 (NEB) and then incubated at 30°C and 250 rpm for 16-18 h. The supernatant of the single culture was used for ELISA as the polyclonal phage ELISA with a 1:1 dilution with 4% skimmed milk in PBS. The strong single binders were sent for sequencing. For recombinant protein ELISA, the RBD or spike proteins were coated on 96-well enzyme-linked immunosorbent assay plates at 50 ng/well. After blocking with 4% skimmed milk in PBS, 50 μL of HuNAbs was added to the plates at 1:5 serial dilutions starting from 10 μg/mL and then incubated for 1 h at 37°C. The plates were washed, and the secondary antibody anti-human IgG-HRP (Invitrogen) was added. 3,3¢,5,5¢- Tetramethylbenzidine liquid substrate (Sigma-Aldrich) was used for color development. Optical density at 450 nm was read on a Varioskan LUX multimode microplate reader (Thermo Fisher Scientific).

Protein expression, purification and Fab production

The antibody VH/VL and constant region genes were amplified and cloned into the expression vectors AbvecIgG and AbvecIgKappa using the NEBuilder® HiFi DNA Assembly Cloning Kit (NEB). The plasmids of paired IgH and IgL genes were cotransfected into the Expi293F expression system (Thermo Fisher Scientific) following the manufacturer's protocol to produce recombinant HuNAbs. Antibodies from cell culture supernatants were purified immediately by affinity chromatography using Recombinant Protein G Agarose (Thermo Fisher Scientific) according to the manufacturer's instructions. The purified HuNAbs were concentrated by an Amicon ultracentrifuge filter device (molecular weight cutoff, 50 kDa; Millipore) to a volume of 0.2 mL in PBS and stored at −80°C. To produce Fab fragments, antibodies were cleaved using Protease Lys-C (Roche) with an IgG to Lys-C ratio of 4000:1 (w/w) in 10mM EDTA, 100mM Tris-HCl, pH 8.5 at 37°C for approximately 12 h. Fc fragments were removed using Protein A Sepharose (GeneScript).

Pseudovirus-based neutralization assay

The neutralizing activity of NAbs was determined using a pseudotype-based neutralization assay as we previously described (Liu et al., 2020a). The pseudovirus was generated through cotransfection of 293T cells with 2 plasmids, pVax-1-S-COVID19 and pNL4-3 Luc_Env_Vpr, carrying the optimized spike (S) gene (QHR63250) and a human immunodeficiency virus type 1 backbone, respectively (Liu et al., 2020a). Viral supernatant was collected 48 h posttransfection and frozen at −150°C. The serially diluted NAbs were incubated with 200 $TCID_{50}$ of pseudovirus at 37°C for 1 h. The HuNAb-virus mixtures were subsequently added into preseeded HEK293T-ACE2 cells. After 48 h, infected cells were lysed to measure luciferase activity using a commercial kit (Promega, Madison, WI). Half-maximal (IC_{50}) or 90% (IC_{90}) inhibitory concentrations of the evaluated HuNAbs were determined by log (inhibitor) versus normalized response–Variable slope using GraphPad Prism 6 (GraphPad Software Inc.).

Please cite this article in press as: Zhou et al., Robust SARS-CoV-2 infection in nasal turbinates after treatment with systemic neutralizing antibodies, Cell Host & Microbe (2021), https://doi.org/10.1016/j.chom.2021.02.019

Neutralization activity of HuNAbs against live SARS-CoV-2

The SARS-CoV-2 focus reduction neutralization test (FRNT) was performed in a certified biosafety level 3 laboratory. Neutralization assays against live SARS-CoV-2 were conducted using a clinical isolate (HKU-001a strain, GenBank accession no: MT230904.1) previously obtained from a nasopharyngeal swab of an infected patient (Chu et al., 2020). Serial dilutions of testing antibodies were conducted, mixed with 50 μL of SARS-CoV-2 (1×10^3 focus forming units/mL, FFU/mL) in 96-well plates and incubated for 1 h at 37°C. Mixtures were then transferred to 96-well plates preseeded with 1×10^4/well Vero E6 cells and incubated at 37°C. After 24 h, the culture medium of the plates was removed and air-dried in a biosafety cabinet (BSC) for 20 min. Cells were then fixed with 4% paraformaldehyde solution for 30 min and air-dried in BSCs again. Cells were further permeabilized with 0.2% Triton X-100 and incubated with cross-reactive rabbit anti-SARS-CoV-2-N IgG (Sino Biological, Inc.) for 1 h at RT before adding Alexa Fluor 488 goat anti-rabbit IgG (H+L) cross-adsorbed secondary antibody (Life Technologies). The numbers of SARS-CoV-2 foci were calculated using the Sapphire Biomolecular Imager (Azure Biosystems).

Antibody binding kinetics and competition with receptor ACE2 measured by SPR

The binding kinetics and affinity of HuNAbs to SARS-CoV-2 spike protein (ACROBiosystems) were analyzed by surface plasmon resonance (SPR, Biacore 8K, GE Healthcare). Specifically, spike protein was covalently immobilized to a CM5 sensor chip via amine groups in 10 mM sodium acetate buffer (pH 5.0) for a final RU of approximately 500. SPR assays were run at a flow rate of 30 mL/min in HEPES buffer. For conventional kinetic/dose-response, a concentration series of HuNAbs IgG1s or Fabs were injected across the spike protein surface for 120 s, followed by a 600 s dissociation phase using a multicycle method. The remaining analytes were removed in the surface regeneration step with injection of 10 mM glycine-HCl (pH 2.0) for 2 × 30 s at a flow rate of 30 μl/min. Kinetic analysis of each reference subtracted injection series was performed using Biacore Insight Evaluation software (GE Healthcare). All sensorgram series were fit to a 1:1 (Langmuir) binding model of interaction. Prior to evaluating competition between antibodies and the human ACE2 peptidase domain, both the saturated binding concentrations of antibodies and ACE2 protein (ACROBiosystems) with immobilized SARS-CoV-2 spike protein were determined separately. In the competitive assay, antibodies at the saturated concentration were injected onto the chip immobilized with spike protein for 120 s until binding steady-state was reached. ACE2 protein at the saturated concentration was then injected for 120 s, which was followed by another 120 s of injection of antibody to ensure the saturated binding reaction against the immobilized spike protein. The differences in response units between ACE2 injection alone and prior antibody incubation reflect the antibodies' competitive ability against ACE2 in binding with spike protein.

Epitope mapping through a yeast surface display system

The antigen library displayed on the yeast surface was constructed by methods described previously (Guo et al., 2015; Zuo et al., 2011). The size of the full-length SARS-CoV-2 spike gene library is approximately 10^6. The conditions of yeast culture and antigen expression induction were described previously (Chao et al., 2006; Guo et al., 2015; Zuo et al., 2011). Galactose-induced yeast library cells (10^6-10^7 cells/test) were blocked by FACS buffer (2% FBS in PBS) for 30 min at 4°C and then incubated with 2 μg screened anti-RBD (SARS-CoV-2) HuNAbs in 50 μL FACS buffer at 4°C for 1 h. After washing twice, yeasts were incubated with AF546-conjugated goat anti-human IgG secondary antibodies (Invitrogen) for another 1 h at 4°C (0.2 μg/test in 50 μL FACS buffer). The fluorescence-positive (PE channel) cells (50k-100k) were sorted into yeast culture media, recultured and reinduced by galactose. The induced yeasts were stained with the same antibodies under the same conditions. The sorted yeast single clones from the second round were verified by FACS. The displayed gene fragments in the plasmids of positive yeasts were amplified by yeast colony PCR and then sequenced. The sequence data were analyzed by Sequencher 5.4.6. (GeneCodes Corp.).

Syrian hamster experiments

In vivo evaluation of HuNAb ZDY20 in an established golden Syrian hamster model of SARS-CoV-2 infection was performed as described previously with slight modifications (Chan et al., 2020a). Briefly, 6- to 8-week-old male and female hamsters were randomized from different litters into experimental groups. The hamsters were obtained from the Chinese University of Hong Kong Laboratory Animal Service Centre through the HKU Centre for Comparative Medicine Research. The experiments were performed in compliance with the relevant ethical regulations. For prophylaxis studies, 24 h before live virus challenge, hamsters were intraperitoneally administered one dose of HuNAb ZDY20 in phosphate-buffered saline (PBS) at 10 mg/kg (n = 4), 5 mg/kg (n = 3), or ZB8 at 4.5 mg/kg (n = 4) or 2-15 at 1.5 mg/kg (n = 4) or control antibody VRC01 at 10 mg/kg (n = 4). On day 0, blood samples were collected from each hamster. Hamsters were then intranasally inoculated with a challenge dose of 100 μL of Dulbecco's modified eagle medium containing 10^5 PFU of SARS-CoV-2 (HKU-001a strain, GenBank accession no: MT230904.1) under intraperitoneal ketamine (200 mg/kg) and xylazine (10 mg/kg) anesthesia. For intranasal administration of HuNAb, each hamster was received 100 μl of PBS containing 10 mg/kg ZDY20 (n = 4) or 4.5 mg/kg ZB8 (n = 4) under intraperitoneal ketamine (200 mg/kg) and xylazine (10 mg/kg) anesthesia at 12 h before 10^5 PFU of SARS-CoV-2 challenge. For the treatment study, each hamster received one 10 mg/kg dose of intraperitoneal HuNAb ZDY20 at 24 h, 48 h, or 72 h (n = 4 per group) after virus challenge. The hamsters were monitored twice daily for clinical signs of disease. Syrian hamsters typically clear virus within one week after SARS-CoV-2 infection (Chan et al., 2020a). Accordingly, animals were sacrificed for analysis at day 4 after virus challenge. Half nasal turbinates, trachea, and lung tissues were used for viral load determination by quantitative SARS-CoV-2-specific RdRp/Hel reverse-transcription polymerase chain reaction assay (Chan et al., 2020c) and infectious virus titration by plaque assay (Chan et al., 2020a). The viral load was normalized by β-actin while the plaque-forming units (PFU) was normalized by mg of tissue extractions based on hamster's bodyweight. For measuring antibody

concentrations in nasal wash, hamsters were treated with Isoflurane lightly, then 200 μL of PBS was injected into one nasal opening while collecting the turbid wash from the other one without any blood contamination.

DNA vaccination in Syrian hamsters

To determine vaccine-induce protection against live SARS-CoV-2, we generated a DNA vaccine using pVAX vector encoding the complete spike protein as we previously described for SARS DNA vaccines (Yi et al., 2005). A dose of 150 μg DNA was used to immunize a group of 6-8 weeks old hamsters (n = 4) at three-week intervals for four time through intramuscular electroporation delivery. The voltage of electroporation was pre-set 60 V in the TERESA DNA Delivery Device (Shanghai Teresa Healthcare Sci-Tech Co., Ltd). Another group of hamsters (n = 3) received equal amount of pVAX vector as a negative control. Serum samples were collected for measuring neutralizing antibodies three weeks after the final vaccination. The vaccinated animals were then challenged intranasally with the same dose as mentioned above at eight weeks after the final vaccination. Animals were consistently sacrificed for endpoint analysis at day 4 after virus challenge.

Histopathology and immunofluorescence (IF) staining

The lung tissues collected at necropsy were fixed in zinc formalin and then processed into paraffin-embedded tissue blocks. The tissue sections (4 μm) were stained with hematoxylin and eosin (H&E) for light microscopy examination as previously described with modifications. For identification and localization of SARS-CoV-2 nucleocapsid protein (NP) in organ tissues, immunofluorescence staining was performed on deparaffinized and rehydrated tissue sections using rabbit anti-SARS-CoV-2-N protein antibody together with FITC-conjugated donkey anti-rabbit IgG (Jackson ImmunoResearch, PA, USA). Briefly, the tissue sections were first treated with antigen unmasking solution (Vector Laboratories) in a pressure cooker. After blocking with 0.1% Sudan black B for 15 min and 1% bovine serum albumin (BSA)/PBS at RT for 30 min, the primary antibody rabbit anti-SARS-CoV-2-N antibody (1:4000 dilution with 1% BSA/PBS) was incubated at 4°C overnight. This step was followed by FITC-conjugated donkey anti-rabbit IgG (Jackson ImmunoResearch) for 30 min and then mounted with 4',6-diamidino-2-phenylindole (DAPI). All tissue sections were examined, and the images were captured with an Olympus BX53 semimotorized fluorescence microscope using cellSens imaging software (Olympus). NP^+ cells per 50 × magnification field were quantified based on the mean fluorescence intensity (MFI) using the ImageJ (https://imagej.nih.gov/ij/download.html).

QUANTIFICATION AND STATISTICAL ANALYSIS

Statistical analysis was performed using PRISM 6.0 or SPSS 26.0. Ordinary one-way ANOVA and multiple comparisons were used to compare group means and differences between multiple groups. Unpaired t test was used to compare group means between two groups only. A P-value < 0.05 was considered to be significant. The figure legends and Methods Materials denotes the number of independent experiments performed, number of animals in each group and specific details on statistical tests.